POLITECNICO
MILANO 1863

SCUOLA DI INGEGNERIA INDUSTRIALE
E DELL'INFORMAZIONE

Aircraft sound modeling through simulation for route optimization

Tesi di Laurea Magistrale in
Aeronautical Engineering - Ingegneria Aeronautica

Author: **Pedro Pablo Javier Zepeda Núñez**

Student ID: 935943
Advisor: Prof. Alberto Luigi Michele Rolando
Co-advisors: Prof. Carlo Emanuele Riboldi, Matteo Crippa
Academic Year: 2021-22

Abstract

Aircraft noise is the most important cause of adverse community reactions related to airport operation and expansion. Control of noise exposure in communities can be achieved in a variety of ways, but its implementation must follow a balanced approach to achieve maximum environmental benefit in the most cost-effective manner. The following work focused on defining a simplified aircraft noise model to study the impact of noise directivity patterns in a trajectory optimization tool called NOICE, which currently models aircraft noise as a single source with spherical spreading.

The literature best practice models suggest regression from actual measurements, but in this case, a simulation approach was tried for the model definition due to the impossibility of accessing these measurements. The simulations were performed using an implemented model in compliance with ECAC Doc. 29 guidelines, used to create airport noise contour maps. Although the goal of this tool is not for simulation purposes, it was possible to define a simplified aircraft noise model that accounts for directivity. Case study analyses focused on Milano Malpensa Airport (LIMC) were then carried out to evaluate the current performance of NOICE against the current noise abatement Standard Instrumental Departure (SID), as well as the sensitivity of its results with respect to the noise model used. The analysis performed determined the importance of a preliminary study of the potential application scenario to define intrinsic constraints. Also, a minimal difference in the optimal route was shown according to the new noise model, achieving a 1.31% decrease in Sound Exposure Level (SEL) over the communities more exposed to noise. Despite the new noise model being approximately 60 times slower than the spherical spreading approximation, the absolute difference in computing time could be negligible and depends on the NOICE optimization program setup.

In general, this work was limited to the non-access of actual measurements. Therefore, the future guidelines focus on developing an embedded system that permits acquiring data to validate the developed models and eventually trying with other approaches like machine learning ones.

Keywords: Aircraft Noise, sound pressure level, ECAC Doc. 29, sound exposure, balanced approach, aircraft noise model.

Abstract in lingua italiana

Il rumore degli aerei è la causa più importante delle reazioni avverse delle comunità legate al funzionamento e all'espansione degli aeroporti. Il controllo dell'esposizione al rumore nelle comunità può essere ottenuto in una varietà di modi, ma la sua implementazione deve seguire un approccio equilibrato per ottenere il massimo beneficio ambientale nel modo più conveniente. Il seguente lavoro si è concentrato sulla definizione di un modello semplificato di rumore degli aerei per studiare l'impatto della direttività del rumore in uno strumento di ottimizzazione della traiettoria chiamato NOICE, che attualmente modella il rumore degli aerei come una singola sorgente con diffusione sferica.
I modelli *best practice* della letteratura suggeriscono la regressione da misure reali, ma in questo caso, è stato provato un approccio di simulazione per la definizione del modello a causa dell'impossibilità di accedervi. La simulazione è stata eseguita utilizzando un modello implementato in conformità con le linee guida ECAC Doc. 29, utilizzato per creare mappe di contorno del rumore aeroportuale. Anche se l'obiettivo di questo strumento non è a scopo di simulazione, è stato possibile definire un modello semplificato di rumore degli aerei che tiene conto della direttività. In seguito, sono state condotte analisi di casi di studio incentrati sull'aeroporto di Milano Malpensa per valutare le prestazioni attuali di NOICE rispetto all'attuale SID di abbattimento del rumore, così come la sensibilità dei suoi risultati rispetto al modello di rumore utilizzato. L'analisi effettuata ha determinato l'importanza di uno studio preliminare del potenziale scenario di applicazione per definire i vincoli intrinseci. Inoltre, è stata mostrata una differenza minima sul percorso ottimale secondo il nuovo modello di rumore, ottenendo una diminuzione dell'1,31% di SEL sulle comunità più esposte al rumore. Nonostante il nuovo modello di rumore sia circa 60 volte più lento dell'approssimazione di diffusione sferica, la differenza assoluta nel tempo di calcolo potrebbe essere trascurabile e dipende dalla configurazione del programma di ottimizzazione NOICE.
In generale, questo lavoro è stato limitato dal mancato accesso a misure reali. Pertanto, le linee guida future si concentrano sullo sviluppo di un sistema incorporato che permetta di acquisire dati per convalidare i modelli sviluppati ed eventualmente provare con altri approcci come quelli basati in *machine learning*.

Parole chiave: Aircraft Noise, sound pressure level, ECAC Doc. 29, sound exposure, balanced approach, aircraft noise model.

Contents

List of Figures

List of Tables

Acronyms

ADS-B	Automatic Dependent Surveillance-Broadcast.
AEDT	Aviation Environmental Design Tool.
ANP	Aircraft Noise Performance.
CPA	Closest point of approach.
DLR	German Aerospace Center.
ECAC	European Civil Aviation Conference.
EMPA	Swiss Federal Laboratories for Materials Science and Technology.
FAA	Federal Aviation Administration.
FDR	Flight Data Recorder.
IATA	International Air Transport Association.
ICAO	International Civil Aviation Organization.
INM	Integrated Noise Model.
ISL	Inverse Square Law.
NPD	Noise Poder Distance.
OASPL	Overall A-Weighted Sound Pressure Level.
PNL	Perceived Noise Level.
SEL	Sound Exposure Level.
SID	Standard Instrumental Departure.

Introduction

Aircraft noise is the most significant cause of adverse community reactions related to the operation and expansion of airports. Beyond the community annoyance, it can negatively impact children learning, disrupt sleep, and increase the risk of cardiovascular disease[1].

A study performed by the International Civil Aviation Organization (ICAO)[2], indicates moderate evidence for cortical awakenings and self-reported sleep disturbance induced by aircraft noise, meanwhile, there is robust evidence for negative effects on children's cognitive skills. The European society of cardiology indicates a high prevalence of cardiovascular diseases like arterial hypertension and coronary heart disease and medication intake in persons exposed to aircraft noise[3].

Despite that bibliography also indicates the necessity of more studies to derive reliable relationships between aircraft noise exposure and negative health impacts, and to address other health diseases like diabetes, obesity, mental health, and birth outcomes; there is evidence of general deterioration of health conditions due to aircraft sound exposure.

International Air Transport Association (IATA) forecasts annual global air passengers growth in the range of 1.5% and 3.8% over the next 20 years [4]. The population affected by noise exposure will increase as the air traffic grows. Currently, these adverse effects affect about 4 million Europeans every year [5]. Therefore, limiting or reducing the number of people affected by significant aircraft noise is a main priority.

ICAO Balance Approach

ICAO is aware of this problem and has set The Balanced Approach to Aircraft Noise Management. This approach identifies the noise problem at a specific airport and analyzes different measures available to reduce noise. The goal is to identify the most cost-effective measures that achieve maximum environmental benefit using objective and measured data [6]. These measures are classified as

Reduction of noise at source

Aircraft noise has been controlled since the 1970s by setting limits for aircraft in the form of standards. These standards set noise limits as a direct function of Maximum Take-Off Weight. In order to obtain certification, aircraft must have noise measures in compliance with ICAO Noise Standards for airplanes[7]. Figure 1 shows the progression of the Noise Standards over time.

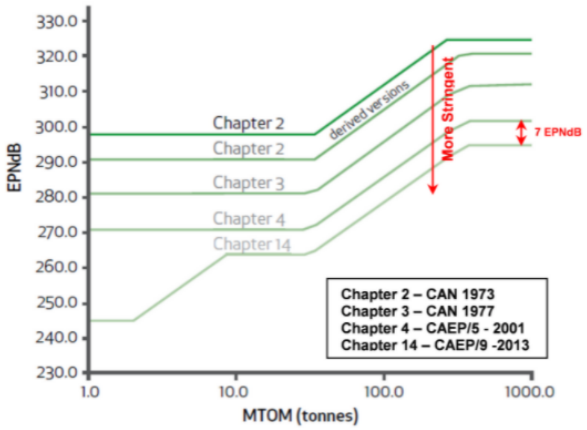

Figure 1: The progression of the ICAO Noise Standards for aircraft

Source: ICAO [7]

Land-Use planning and management

Land-use planning and management are addressed in the feasibility studies for new airports or the expansion of existing ones. Therefore analyzes of noise impact on the communities due to potential positions and routes are performed. It also accounts to ensure that the activities nearby airports are compatible with aviation. Its main goal is to minimize the population affected by aircraft noise[8].

Noise abatement operational procedures

Noise abatement operational procedures studies and propose procedural solutions that are safe and cost-effective, to reduce noise exposure in communities close to current airports. The possibilities include preferential runways and routes with abatement procedures for take-off and landing. In all cases, procedures must give priority to safety consideration [9].

Operating restrictions

This measure mainly focuses on the phase-out of Non-Noise Certified aircraft and has already taken place in many ICAO contracting states. Other possible operational restrictions include curfews, night-time restrictions, noise quotas, etc. These restrictions are described in Chapter 7 of ICAO Doc 9829[10].

Thesis' contribution

Mathematical models and optimization tools are currently being studied and developed to generate air routes that minimize noise exposure in communities close to airports. These tools can address ICAO's land use planning and management, and noise abatement procedures measurements to achieve maximum environmental benefits. This thesis will focus on improving the NOICE program capabilities [11].

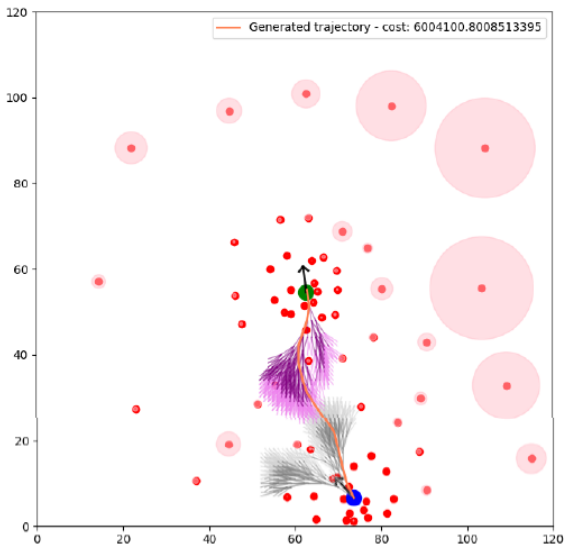

Figure 2: Minimal noise exposure route from the optimization tool

Source: M.Gullo [11]

NOICE is a program currently in development to reduce noise exposure through trajectory optimization. It is based on non-linear programming and relies on A*, a graph-search algorithm. This algorithm exploits and evaluates air routes from point A to point B to reduce the noise exposure over sensible receptors on the ground. It is focused on take-off and landing procedures. An example of the model results is reported in fig. 2.

In NOICE, the noise source is modeled as a monopole with spherical spreading in 2D.

Figure 3 shows the noise level perceived by a sensitive receiver, where horizontal coordinates correspond to the aircraft position with respect to the receiver, meanwhile vertical coordinates correspond to the noise value. Getting close to the receptor quadratically increases the noise level following the Inverse Square Law (ISL), i.e., is proportional to $\frac{1}{r^2}$ with r equal to the distance between aircraft and sensitive receiver.

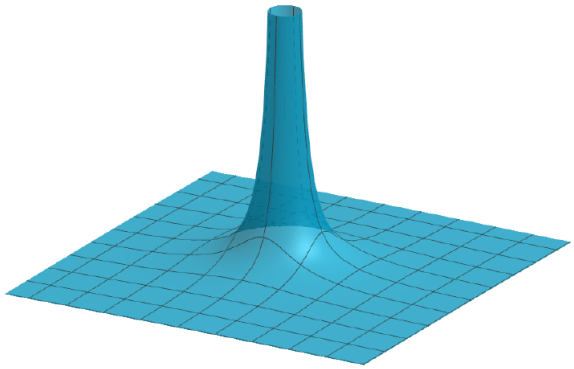

Figure 3: Current 2D noise propagation model

Source: M.Gullo [11]

One of the main drawbacks of the current tool is the sound model used. As it is a 2D, the noise level for a flyover case is non-negligible even if the airplane is at a considerable vertical distance from the sensitive receiver. Also, this model does not account for sound directivity propagation, which can be a crucial factor in obtaining the optimal route. Improving the optimization tool to account for the vertical profile and analyze a 3D scenario is also mandatory despite it not part of this work.

As previously mentioned, the scope of this thesis is to improve the capabilities of the tool, and this work will address the noise model representation for route optimization. Therefore, the goal is to obtain a simplified noise model that accounts for directivity patterns and vertical distance to make a robust route optimization tool. This simplified noise model should be sufficiently simplified not to worsen the optimization tool's execution time. Eventually, the study of the effectiveness of the introduced noise model and the impact on the generated optimized routes.

1 | Theoretical Framework

This chapter aims to introduce a general overview of sound and noise to understand future explanations in this thesis.

1.1. Sound

Sound is a physical phenomenon that consists of a vibration that propagates as an acoustic wave and generates pressure variations due to adiabatic compression and expansion. This wave is transmitted through a gas, liquid, or solid medium. In the atmosphere, the sound is a rapid variation of the pressure around the value of atmospheric pressure at a certain point.

A sound event, as reported on fig. 1.1, is characterized by the acoustic wave's frequency, wavelength, and amplitude, and these values depend on the distance between the source and the receiver. The human ear can perceive acoustic waves on average between 20Hz to 20kHz.

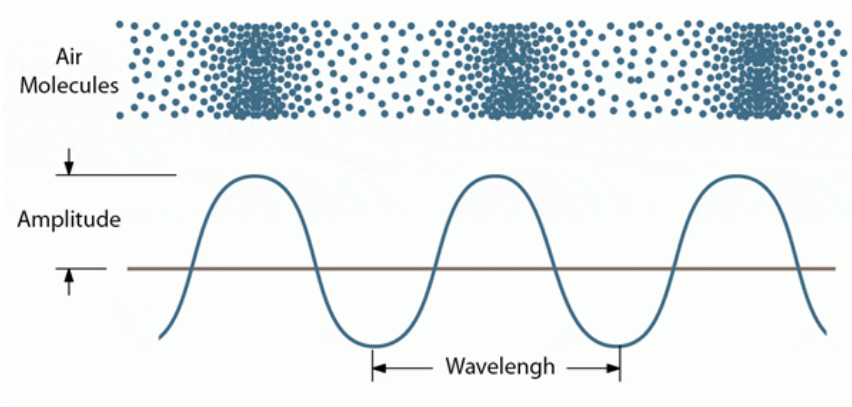

Figure 1.1: Sound wave physics

Source: Soundproofing Company [12]

1.2. Sound quantification

As a physical phenomenon, sound can be quantified in diverse valuable forms. The measure of interest depends on the final analysis and the difficulty of measuring. Below are the three main ways of quantizing sound.

Sound pressure

Sound pressure is a scalar quantity used to indicate the amplitude level at a specific location in space. It corresponds to the deviation from the atmospheric pressure caused by the acoustic wave. It depends on the distance the measure is taken from the source and the atmospheric environment.

Sound power

Sound power is the rate at which sound energy is emitted from a source per unit of time. This last produces sound pressure variations at some distance from the source. The sound power characterizes the noise source as it is independent of distance.

Sound intensity

Sound intensity is the sound power per area unit and indicates the flow of sound through a specific area in a direction. Therefore, it has a level and direction. Sound intensity is related to sound pressure and power as:

$$Sound\ intensity = Sound\ pressure \cdot Particle\ velocity$$

$$Sound\ intensity = \frac{Sound\ power}{Area}$$

All the measurements mentioned before are commonly reported in decibels. A decibel is not a unit of measure but a logarithmic ratio between a reference value and the measured one. Hence, sound measurements are reported in levels, such as sound pressure level, sound power level, or sound intensity level. Table 1.1 reports the reference values.

Measurement	Measurement unit	Reported unit
Sound pressure	Pa (Pascal)	dB (ref $= 20 \cdot 10^{-6}$ Pa)
Sound power	W(Watts)	dB(ref $= 1 \cdot 10^{-12}$ W)
Sound intensity	W/m^2(Watts/area)	dB(ref $= 1 \cdot 10^{-12}$ W/m^2)

Table 1.1: Reference values for sound representations

1.3. Noise spectrum and weighing

A sound that exhibits a perfectly sinusoidal pressure variation is called a tone, and its constant frequency characterizes it. On the other hand, complex and non-periodic sound waves have a broadband frequency spectrum.

The noise produced by the different sound sources in an airplane can have both characteristics. However, when adding the contribution of all the sources, an acoustic wave with a wide frequency band, commonly called broadband, is presented. Figure 1.2 reports different signals and their spectral decomposition, where it can be observed a broadband noise.

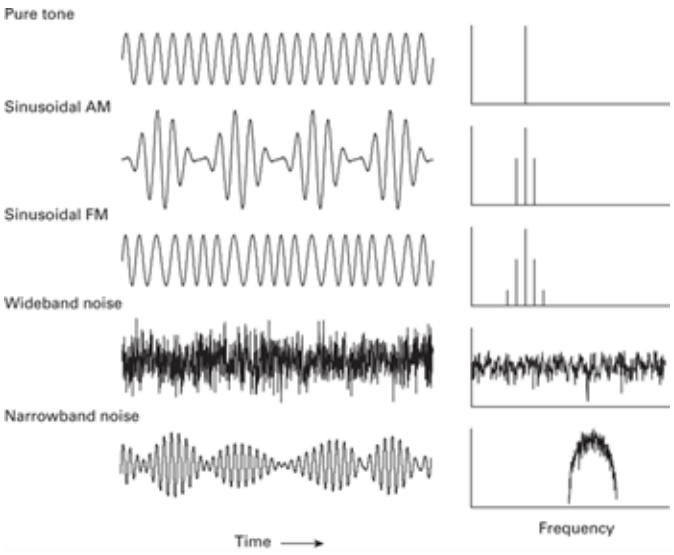

Figure 1.2: Different sound waves comparison

Source: C. J. Plack [13]

The study of sound, especially for human response, is performed in octaves. Octaves or octave bands are a group of frequencies that helps quantify how humans distinguish between frequencies and represent overall energy over a specific frequency range. Humans can hear noise in the frequency range of 20 to 20kH; in this frequency band, the human ear reacts differently depending on the frequency spectrum. Higher accuracy can be achieved

considering even smaller frequency ranges, as 1/3 octave bands reported in fig. 1.3.

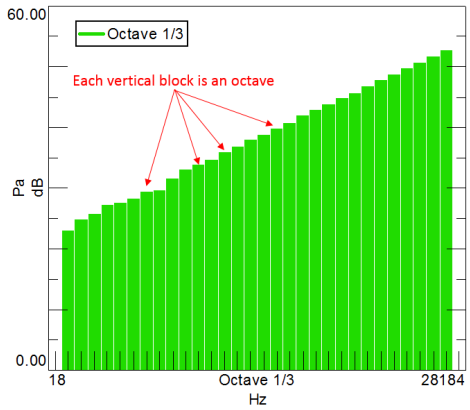

Figure 1.3: 1/3 Octave bands

Source: Siemens [14]

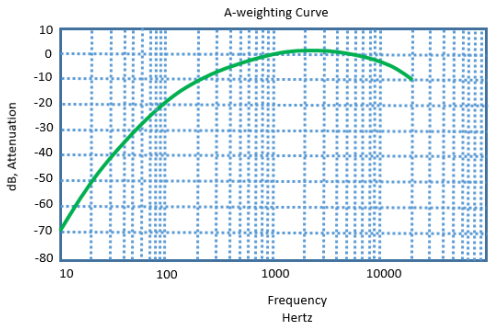

Figure 1.4: A-weighting curve

Source: Siemens [15]

Noise measurements are often weighted with an A-weighting filter to mimic the effects of human hearing. This filter corresponds to a curve that alters the recorded sound pressure levels to match the human ear's perception. As reported in fig. 1.4, this curve attenuates the measurement below 1000Hz and above 6000Hz, and amplifies the dB measurements between the range of 1000Hz to 6000Hz.

Figure 1.5 presents a comparison of the A-weighted sound pressure level (dBA) depending on different noise sources and distances.

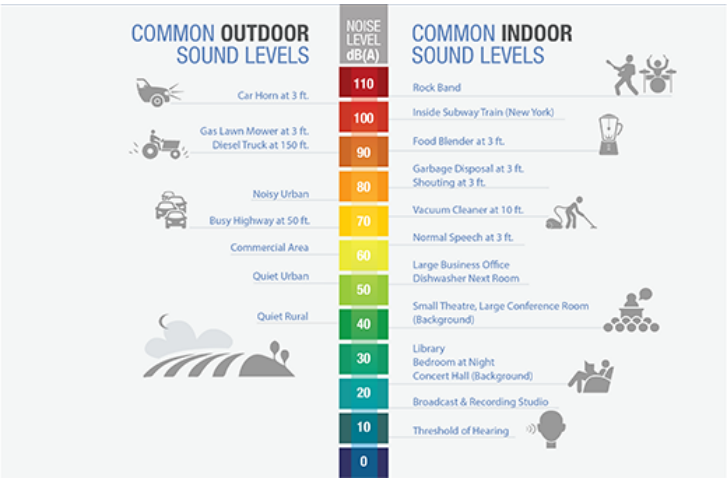

Figure 1.5: A-Weighted sound level comparison on different sources

Source: FAA [16]

1.4. Aircraft noise measurements

Different noise measurements can be used to study an aircraft event. Therefore, measurements are classified onto single noise events metrics and exposure-based descriptors.

1.4.1. Single event metrics

An event can be measured at a specific position by recording the sound level L as a function of time t. Then, the noise level time history of the specific event, or flyover, can be characterized by two parameters: the maximum sound level L_{max} and the sound duration t, in which L is expressed as an A-weighted sound pressure level. If its tone is corrected [17], the measure is called Perceived Noise Level (PNL).

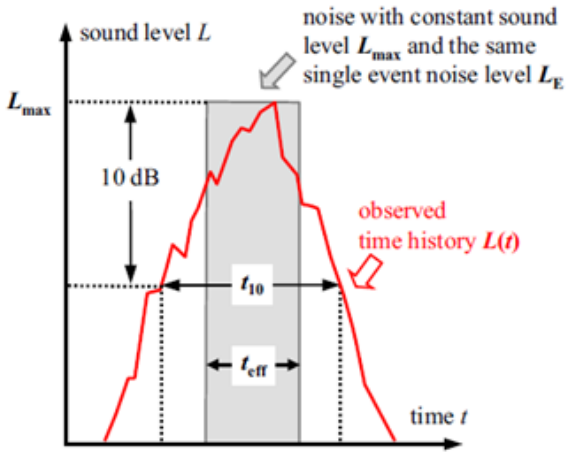

Figure 1.6: Sound-level time history for single event

Source: U. Isermann and L. Bertsch [18]

As reported in fig. 1.6, there are two main definitions for the event duration. The so-called 10dB downtime t_{10}, where $L(t)$ is at most 10dB below the maximum level, and the effective duration t_{eff}, is defined by the eq. (1.1), where t_1 and t_2 define the period of time in which the noise can be identified[18].

$$\int_{t_1}^{t_2} 10^{L(t)/10} = t_{eff} \cdot 10^{L_{max}/10} \tag{1.1}$$

On the other hand, the single event sound exposure level is defined as shown in eq. (1.2). It corresponds to a normalized integral measure representing the total energy exposure that depends on the perceived level and duration. Then, the SEL is defined as the single

event sound exposure level with normalization time t_0 of 1s, see eq. (1.3).

$$L_E = 10 \cdot \log\left(\frac{1}{t_0}\int_{t_1}^{t_2} 10^{L(t)/10}\right) = L_{max} + \log\left(\frac{t_{eff}}{t_0}\right) \tag{1.2}$$

$$SEL = L_{max} + \log\left(t_{eff}\right) \tag{1.3}$$

1.4.2. Cumulative noise metrics.

General exposure studies for overall community annoyance focus on long-term multiple-events average measurements that penalize noise events at a specific time of the day. Generally, the equivalent continuous sound level L_{eq} is defined according to eq. (1.4). It is the basis for average sound level measures that penalize depending on day time, as the average A-weighed sound level reported on eq. (1.5), in which τ_i is the penalty factor and T the averaging time, usually 15hr a day [19].

$$L_{eq} = 10 \cdot \log\left(\frac{t_0}{T_c}\sum_{i=1}^{N} 10^{L_{AE_i}/10}\right) \tag{1.4}$$

$$L_{AeqT} = 10 \cdot \log\left(\frac{t_0}{T_c}\sum_{i=1}^{N} \tau_i 10^{L_{AE_i}/10}\right) \tag{1.5}$$

This work will focus on single event measures because the main goal is to obtain a simplified model that does not worsen the algorithm execution time, although exposure averaged metrics are derived from multiple single events analyzes.

2 | State of the art

The study of the aircraft noise is divided in two main fields. The first field corresponds to the source, i.e., how the noise is produced regarding the different sources present in the aircraft configuration. The second one, corresponds to the sound propagation, i.e., how the sound wave travels through the medium, in this case the atmosphere. Both fields have their own theory and can be studied together or separately.

2.1. Aircraft noise sources

Aircraft noise sources can be divided into two groups, the air-frame one and the engine one. Both groups have different components and generation mechanisms that contributes to the overall sound power level. Table 2.1 and Table 2.2 shows the main noise sources according to [20], these tables include also the noise generating mechanism, the conditions under which important and the level of theoretical understanding.

Noise Source	Generating mechanism	Condition under which important	Theorical undestanding
Landing gear	Broadband	Low engine setting (final approach)	Medium
Flaps	Broadband	Low or idle engine(approach)	Good
Slats	Broadband	Low or idle engine(approach)	Medium
Lift and control surfaces	Broadband	Low engine setting, clean configuration(far approach)	Medium
Spoiles and speed brakes	Detached flow	Low engine setting (complete approach)	Low
Kruegger	Not understood	Heavy use of spoiler	Low

Table 2.1: Airframe main noise sources

Source: L. Bertsch, D. G. Simons, and M. Snellen [20]

Noise Source	Generating mechanism	Condition under which important	Theoretical undestanding
Fan	Tonal and broadband	Always	Medium for Tones Low for Broadband
Jet	Turbulent mixing and shock noise	Take-off	Good Subsonic Medium Sonic
Combustion	Broadband	Approach Departure Side-line	Low
Turbine	Tonal and broadband	Approach Departure After cut-back	Low-Medium
Compressor	Tonal and broadband	Approach Departure After cut-back	Medium

Table 2.2: Engine main noise sources

Source: L. Bertsch, D. G. Simons, and M. Snellen [20]

2.2. Aircraft noise propagation

As previously mentioned, a sound wave corresponds to a vibration that propagates through a medium, in this case the atmosphere. Propagation of the sound wave through the atmosphere depends on a variety of factors which are briefly described below.

Geometrical spreading is independent on frequency and plays a major role in sound propagation. It causes the the sound intensity to diminish as $1/R^2$, where R is the distance from the source [21]. On the other side, the exponential attenuation of sound due to heat conduction, viscosity and molecular relaxation loses, converts a proportion of sound energy into heat as it travels through the air. The atmospheric attenuation becomes significant at high frequencies and long distances so air acts as a low-pass filter at larger distances [22].

Reflections from the ground effects, specially for elevated sound source, are the result of interference between sound travelling directly from the observer and sound reflected from the ground to the observer. Refraction by vertical gradients of wind and temperature in the atmosphere, plays a role non negligible in the atmospheric boundary layer. Part of the noise propagation components are graphically presented in fig. 2.1.

2.3. Noise models

Currently, there are diverse approaches for studying and estimating aircraft noise. This is due to the different levels of theoretical understanding of the noise generation mechanisms. Therefore, different levels of modeling capabilities exist, and they depend on the

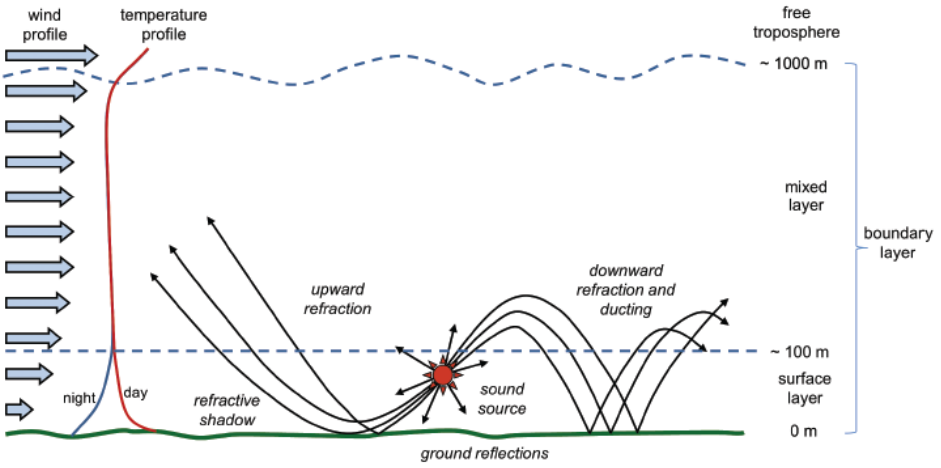

Figure 2.1: Sound propagation mechanism

Source: K. Attenborough [22]

accuracy and the application. Models are used for various applications, such as studying and analyzing new aircraft configurations, estimating noise contours around airports, or evaluating noise mitigation procedures.

The current simulation and estimation procedures used to study noise generation and propagation can be categorized as follows:

Fully numerical With this approach, the source and the propagation mechanisms are studied and simulated simultaneously in one Computational Fluid Dynamics and Computational Aeroacoustics run. These type of simulations require vast computational domain to capturing the sound source and propagation behaviours.

Step numerical With this approach the source and the propagation are studied in different steps. The aerodynamic flow is calculated first for the region where the origins of the sound are expected to be located. Based on post processing the aerodynamic field results, the sound sources are calculated.

Semi-Analytical Comprises all approaches where the flow and acoustic filed are derived analytically, the source can be treated as a combination of monopoles, dipoles and quadropoles. Instead, the sound propagation can be estimated solving a Green function or Ray Theory function. Currently, these type of models are combined with other approaches, preferentially empirical ones.

Empirical These methods are based on databases containing measured acoustic data and estimates the noise level applying corrections to the databases measurements.

Within this line, latest research is seeking to apply machine learning models to estimate sound level on the ground [23].

Table 2.3 present main of the current models classified according to the previously described groups.

Model name	Origin	Type
AEDT	FAA	Empirical
IESTA	ONERA	Empirical
AzB	DLR	Empirical
ANCON2	CAA	Empirical
ECAC Doc. 29	ECAC	Empirical
NORTIM	Norway	Empirical
IMPACT	Eurocontrol	Empirical
sonAIR	EMPA	Semi Analytical
ANOPP	NASA	Semi Analytical
PANAM	DLR	Semi Analytical
FLIGHT	Filippone	Semi Analytical
FLULA 2	EMPA	Semi Analytical
DNS	-	Full numerical
LES	-	Full numerical
U-RANS	-	Full numerical
Piano	DLR	Acoustic numerical
UPACK-LES	JAXA	Acoustic numerical

Table 2.3: Noise models comparison

Source: L. Bertsch, D. G. Simons, and M. Snellen [20]

Models reported in table 2.3, have been developed for different porpuses and by different agents. Some of them are used for noise exposure studies and can be purchased commercially, meanwhile other models have been developed by governmental research groups for internal use only. Fully-numerical and acoustic numerical models have research goals and they use to be the more sophisticated ones, others corresponds to general guidelines or procedures for noise modelling, like ECAC Doc. 29 [24].

As dictated by the EU Directive 2002/49/EC [25], European airports should produce noise emission maps and prepare actions plans for flight management for noise exposure assessment. Also, according to EU Directive 2009/12/EC [26] airports operator are allowed to make charges to airlines which do not comply with specific standards.

To address noise impact analysis for a defined flight-path over an airport scenario, there are three main approaches.

Closest point of approach (CPA) As the name indicates, for a defined route and sensitive receiver on ground, it measures the sound pressure level at the closest point of approach. They were developed before adoption of time-integrated noise metrics and rely on L_{max} metrics.

Segmentation This approach is a generalization of CPA approach, in which the entire flight-path to be analyzed is discretized in straight segments, which calculate the separate contributions to L_E from all noise-significant flight path segments.

Simulation This approach describe the flight-path as a series of discrete points in the space. The level-time-history at any observer location is then constructed by calculating the sound radiated to each receiver. This approach presents two main disadvantages. Heavy computer processing demand and the need of very detailed input data.

For aircraft noise impact assessment, the most common used models are semi-analytical and empirical ones based on segmentation approaches. Empirical models are commonly called *best practice models* and they can, depending on the defined scenario, assess noise exposure on communities close to airports through noise contours.

2.4. Noise impact assessment models

The majority of best practice models are compliant with the guidelines given by ICAO Doc. 9911 [27] in the US and European Civil Aviation Conference (ECAC) Doc. 29 [24] in Europe. Both guidelines are based on segmentation analysis and give as final output cumulative noise metrics and noise contours.

One of the most widely used models for noise contours corresponds to the Integrated Noise Model (INM) developed by the Federal Aviation Administration (FAA). INM is a commercial tool compliant with the ICAO directives [28]. The tool relies on the so called Noise Poder Distance (NPD) curves that for a given distance and required power, estimates the noise level which is corrected according to environmental and geometric factors. FAA has also developed the Aviation Environmental Design Tool (AEDT) which is a upgrade of the INM tool that account for atmospheric pollution and fuel burn [29].

On the other hand, Swiss Federal Laboratories for Materials Science and Technology (EMPA) has developed FLULA 2. It is a prediction methodology based on measured aircraft noise radiation directivity patterns to calculate single event aircraft noise [30], is based on an extensive noise database which was established based on measurements

under real air traffic operations [31]. FLULA2 also exploits the mathematical physics application of spherical harmonics [32].

EMPA has also developed a more robust model sonAIR, which comprises of a source model describing in detail the sound emission and directivity as a function of flight configuration [33]. This source model is combined with the sound propagation model sonX, also developed by EMPA, and simulates a flight-path according to a time-step procedure. As it is a simulation approach, it requires more input data and its performance is limited to availability of Flight Data Recorder (FDR) data [34].

German Aerospace Center (DLR) has developed his own model as one tool for the enforcement of the revised German Act for Protection against Aircraft Noise[35]. It is a best-practice model based on segmentation approach. It considers separately the noise source and its propagation. It describes the source by sound power levels with a triple of directivity factors for each octave band. These data are derived from measurements, in most cases from noise monitoring stations at German airports. For the propagation, it considers geometrical spreading, atmospheric absorption and ground attenuation effects.

Different national agencies or laboratories have developed their own tools that comply with ECAC Doc. 29. English ANCONN program is used for annual generation of noise emission maps. This last model is continuously updated with trajectory and sound pressure level data. Simmilar tools have been developed by Norway, with NORTIM tool; or France with IESTA.

2.5. Noise directivity

The models previously described accounts for aircraft noise directivity from different approaches.

ECAC Doc. 29 guidelines considers lateral directivity correction factors for engine installation. This correction depends on the inclination angle between observer and noise source as reported in fig. 2.2. For longitudinal directivity it only account for Start-Of-Roll correction, further details of this procedure are given in chapter 3.

In the case of FLULA 2, this model correct the noise level measurement spectrum $L_{d,i}$ to a reference distance $L_{R,i}$ according to Equation (2.1), where d is the distance where the measurement was taken and R the reconstruction distance. This correction is frequency dependant for the atmospheric attenuation (α_i, $\alpha_{0,i}$), therefore the correction is performed by each one-third-octave i.

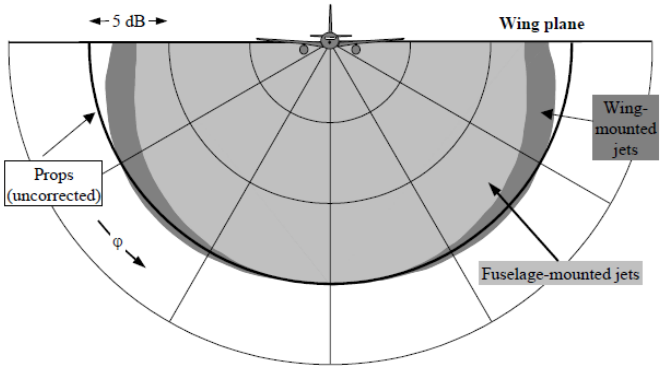

Figure 2.2: ECAC Doc. 29 lateral directivity correction due to engine installation

Source: ECAC [36]

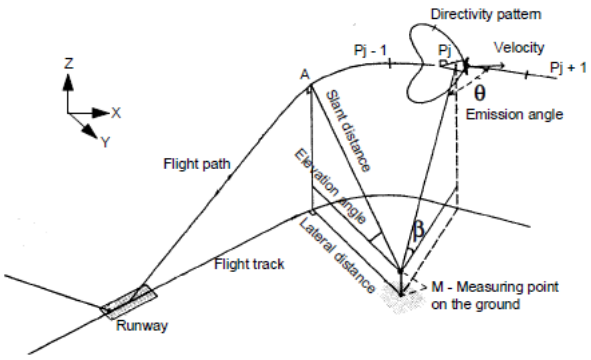

Figure 2.3: FLULA 2 model geometric definitions

Source: Pietrzko, Stan and Bütikofer, Rudolf [30]

$$L_{R,i} = L_{d,i} + 20\log\left(\frac{d}{R}\right) + \alpha_i \cdot d + \alpha_{0,i} \cdot R \tag{2.1}$$

Subsequently, to derive the desired directivity pattern at some radius R, it uses least-squares fitting according to eq. (2.2) where R corresponds to the reference propagation or slant distance for spectrum reconstruction and θ the radiation angle as reported in fig. 2.3. This equation estimates the OASPL considering spherical spreading and atmospheric attenuation effects. Therefore, it is necessary to estimate 32 parameters from measurements according to Equation (2.3). Figure 2.4 shows the Overall A-Weighted Sound Pressure Level (OASPL) for a MD11 aircraft from FLULA 2 model.

$$L(R,\theta) = \sum_{k=0}^{7} A_k(R) cos(\theta)^k \tag{2.2}$$

$$A_k(R) = H_{k1} \cdot 20\, log(R) + H_{k2} + H_{k3} \cdot R + H_{k4} \cdot R^2 \tag{2.3}$$

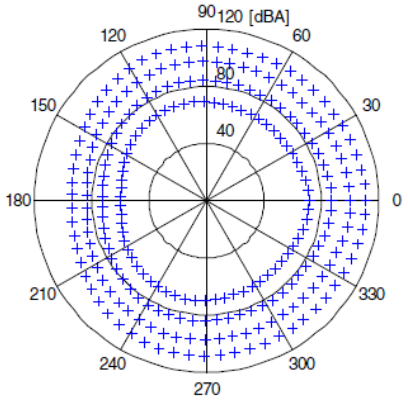

Figure 2.4: Polar plot of OASPL for a MD-11 from FLULA 2 model at R = 100, 305, 1000 and 3000 [m], respectively

Source: Pietrzko, Stan and Bütikofer, Rudolf [30]

AzB model instead, considers directivity by adding a correction with a triple of directivity factors $R_n = \{a_1, a_2, a_3\}$ as eq. (2.4), which are derived from measurements and they are use to predict spectral directivity by a series expansion over the cosine of θ, which is defined between the longitudinal aircraft axis and the propagation vector as showed in fig. 2.3. Figure 2.5 shows source noise directivity pattern from AzB model for aircraft category similar to A320 or B737-300.

$$D_{I,n}(\theta) = 3 \cdot [a_1 \cdot cos(\theta) + a_2 \cdot cos(2\theta) + a_3 \cdot cos(3\theta)] \tag{2.4}$$

Latest models that accounts for noise directivity correspond to semi-empirical ones and they need as inputs further operating parameters. SonAIR model accounts for spectral three-dimensional directivity [37] and the noise source is modeled as eq. (2.5), where Ma corresponds to Mach number, ρ air density, FH flaps settings, LG landing gear settings, SB speed brakes settings and $Proc$ the procedures adjustments. The directivity correction is applied with a second order Fourier series as eq. (2.6)where factors k, l, m, n are found by regressions and N_1 corresponds to engine rotational speed.

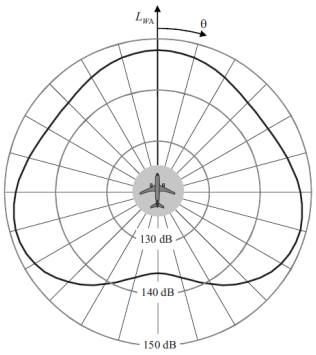

Figure 2.5: AzB source directivity pattern for aircraft group S5.2 (e.g. B737-300, A320).

Source: Isermann, Ullrich and Vogelsang, Berthold [35]

$$L_{em}(f) = \hat{L}(lMa, l\rho, FH, LG, SB, Proc) + \Delta L_\theta(\theta, N) \tag{2.5}$$

$$\Delta L_\theta(\theta, N) = (k_{e,j} \cdot cos(\theta) + l_{e,j} \cdot sin(\theta) + m_{e,j} \cdot cos(2\theta) + n_{e,j} \cdot sin(2\theta)) \cdot \left(1 + N_1 + N_1^2\right) \tag{2.6}$$

3 | ECAC Model

According to ECAC Doc. 29 guidelines, a model has been implemented to compare the current and subsequent results of NOICE. This chapters summarizes ECAC Doc. 29 characteristics and implementation.

3.1. Model's scope

The ECAC Doc. 29 provides comprehensive guidance for calculating aircraft noise exposure levels and noise contours for noise assessment. Therefore, it is not a program itself, but it presents the model guidelines for its implementation. As previously mentioned, it follows a segmentation approach and estimates the noise level following a fully-empirical method using the Aircraft Noise Performance (ANP) database. It is necessary to clarify that this guide is not specified for the study of single events but rather for the study of the impact of multiple events.

ECAC Doc. 29 is divided into three Volumes. The first one introduces Doc. 29 and describes the main noise computation concepts. The second Volume [36] presents all the modeling guidelines, from the trajectory definition to noise computation and the realization of the noise contours map. Finally, the third Volume [38] defines a set of reference cases to validate the implemented relationships.

The general guidelines reported in Volume 2 is divided into two sub-routines. The first one corresponds to the trajectory definition, in which the segments and their characteristics are defined for the noise computation. The second one corresponds to the noise computation procedure and its post-processing analysis.

3.2. The ANP database

The ANP database is an international data resource compliant with ICAO Doc. 911 directiveness. EUROCONTROL hosts it, and it is free to access after registration on the official ANP webpage [39]. As the acronyms suggest, this database contains Air-

craft, Noise, and Performance characteristics for various commercial and general aviation aircraft.

The database provides the NPD curves for the noise computation. This curve corresponds to noise levels at ten slant distances depending on the engine power. It also offers Spectral Classes for adjustment to non-reference atmospheric conditions.

It also contains different performance indicators such as engine, aerodynamics coefficients, and standard operational take-off and landing procedures. Therefore, all the database info is useful to define flight profiles for trajectory definition.

3.3. Trajectory definition

To estimate the noise components is mandatory to define a trajectory that describes aircraft motion in time and space. The flight path is represented as continuous straight segments with the engine thrust or power characteristics. The trajectory definition can be addressed from two approaches: a synthesis from procedural step data or an analysis of measured flight profile data.

3.3.1. Synthesis from procedural steps

In general, each segment has to be defined by the geometrical coordinates of its endpoints and the associated speed and engine parameter. The procedural synthesis is divided into the ground track and the flight profile definitions. Both definitions will eventually combine to create a unique flight path.

Ground track

Ground track corresponds to the flight path projection onto the ground, and it is defined by a continuous sequence of straight segments. For the case of turns, they are discretized through different straight segments. The ground track is generally defined as a sequence of straight or turn indications. Table 3.1 shows an example of ground track definition for a take-off procedure.

The model guidelines considers 3D Cartesian coordinates with origin in brake release point. The x-axis is aligned with the runway; meanwhile, the z-axis describes the aircraft's altitude. Figure 3.1 shows an approximated ground track projection for a departure from Runway 35L of Milano Malpensa Airport according to SID.

Segment type	Length [ft]	Radius [ft]	Heading change [°]	Transition heading change [°]	Turn direction
Straight	16000				
Turn		9114	20	5	Left
Straight	31600				
Turn		9114	80	5	Left
Straight	30000				

Table 3.1: Departure 35L ground track at Milano Malpensa Airport

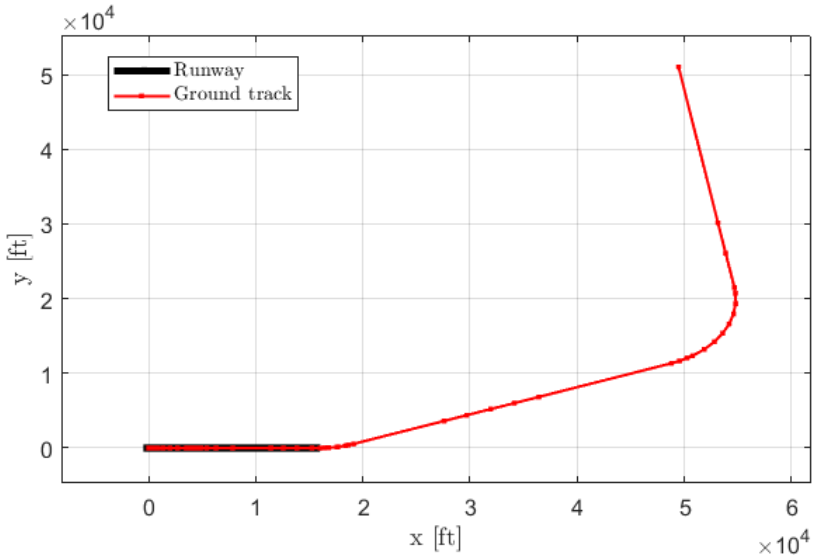

Figure 3.1: Milano Malpensa 35L Ground track departure

Flight profile

The flight profile describes aircraft motion in terms of altitude, speed, power. Its definition relies on the default departure and arrival procedures defined in the ANP database, which defines a sequence of steps for both cases. In the case of departure, the steps correspond to take-off, acceleration, and climb. The arrival includes the descent, landing approach, touchdown, and deceleration phases.

Each of the steps previously mentioned represents a specific aircraft configuration of power settings, flap settings, and speed, with which later the necessary inputs can be determined to estimate the sound level. Doc. 29 Volume 2 presents all the relationships to determine the flight profile, from standard procedures, as a function of the distance traveled on the ground s. Figure 3.2 shows the flight profile for an Airbus 320 departure

After defining ground track and flight profile, both systems are merged as a unique trajectory. The ground track synthesis gives x and y coordinates in the ground plane. Meanwhile, the flight profile gives altitude (z), speed(V), and engine power (P).

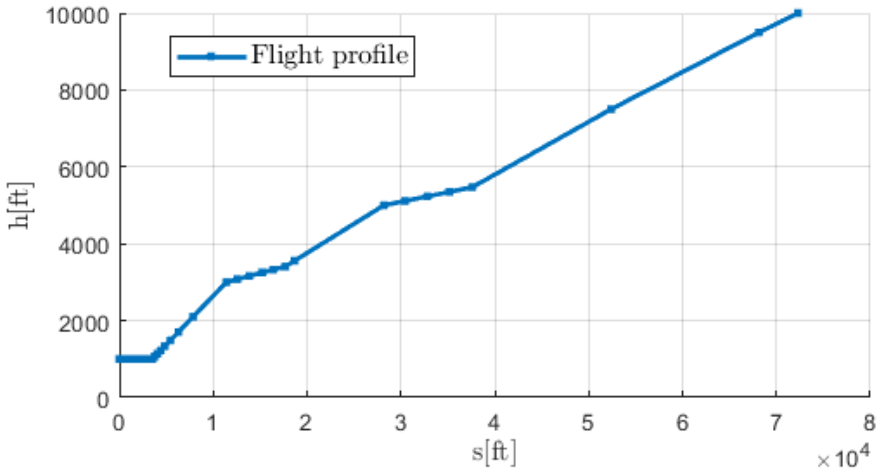

Figure 3.2: A320 default flight profile procedure

The link between both sets of discrete points corresponds to the distance along with the ground track s. The interpolation relationships of eq. (3.1) are used to define the ground coordinates to the flight profile points. The subscripts 1 and 2 represent the initial and final segment points.

$$\begin{aligned} x &= x_1 + \frac{s - s_1}{s_2 - s_1}(x_2 - x_1) \\ y &= y_1 + \frac{s - s_1}{s_2 - s_1}(y_2 - y_1) \end{aligned} \tag{3.1}$$

In the same way, eq. (3.2) expressions are used to set altitude, speed, and power settings for the defined ground points.

$$\begin{aligned} z &= z_1 + \frac{s - s_1}{s_2 - s_1}(z_2 - z_1) \\ V &= \sqrt{V_1^2 + \frac{s - s_1}{s_2 - s_1}(V_2^2 - V_1^2)} \\ P &= \sqrt{P_1^2 + \frac{s - s_1}{s_2 - s_1}(P_2^2 - P_1^2)} \end{aligned} \tag{3.2}$$

After matching both methods, it is possible to define the bank angles (ε) for turns. They are defined as a function of the ground speed (V_g), turn radius (r), and gravity acceleration (g) according to eq. (3.3).

$$\varepsilon = \tan^{-1}\left(\frac{V_g^2}{rg}\right) \tag{3.3}$$

Finally, the flight trajectory is defined for the noise level calculation, see fig. 3.3. The list of inputs for the noise computation corresponds to:

- x, y, z, s
- ϵ
- V
- P

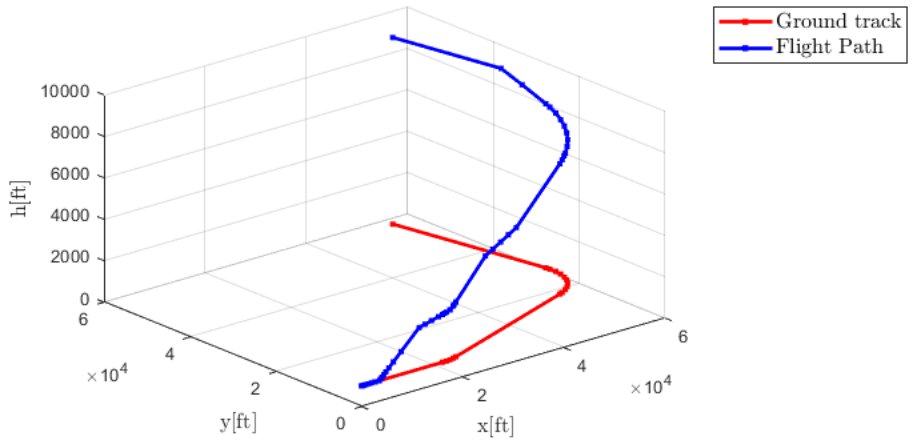

Figure 3.3: A320 Milano Malpensa departure flight path

3.3.2. Synthesis from flight data

Another way to define the trajectory corresponds to radar data processing. If position data and time are available, it is possible to determine the entire flight path. From the relationships presented in Volume 2 is straightforward to obtain thrust from altitude and speed change.

Generally, accessing this type of detailed data is difficult, but currently, online radar applications, such as FlightRadar24[40] give the necessary data to process and define flight paths. An example of trajectory definition from flight data synthesis is presented in fig. 3.4.

3.4. Noise computation

Figure 3.5 reports NPD curves from the ANP database. These curves tabulate noise levels L as a function of propagation distances (d) and power settings (P). The tabulated

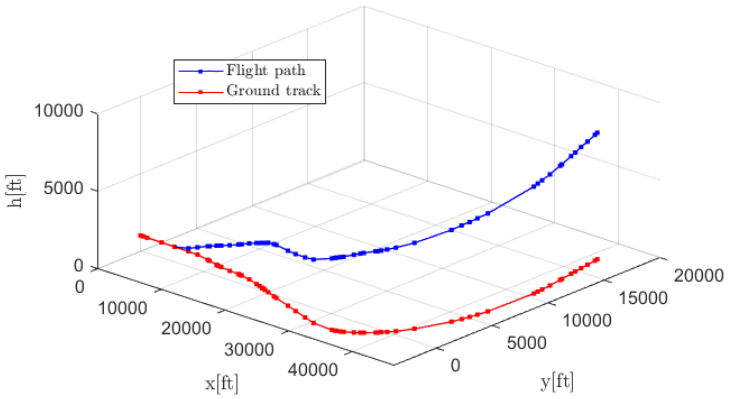

Figure 3.4: Radar trajectory from flight VY6329 03/15/2022

noise levels correspond to the L_{max}, and L_E, reported at reference speeds V_{ref} assuming an infinite straight flight path. The NPD curves represent a look-up table; therefore, as the values are reported for certain combinations of d, P; noise levels can be obtained by double interpolation. First for power and then for distance, as reported in eq. (3.4). In the same way, extrapolation can be performed if the desired d, P combination is out of the range.

$$\begin{aligned} L(P) &= L\left(P_i\right) + \frac{L\left(P_{i+1}\right) - L\left(P_i\right)}{P_{i+1} - P_i} \cdot \left(P - P_i\right) \\ L(d) &= L\left(d_i\right) + \frac{L\left(d_{i+1}\right) - L\left(d_i\right)}{\log d_{i+1} - \log d_i} \cdot \left(\log d - \log d_i\right) \end{aligned} \tag{3.4}$$

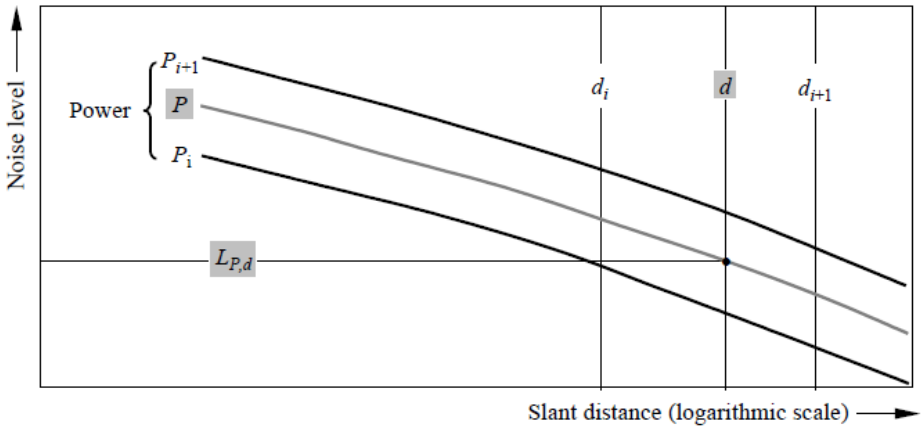

Figure 3.5: Interpolation in noise-power-distance curves.

Source: ECAC [36]

For single event noise computations, ECAC Doc. 29 reports the relationships of eq. (3.5) to estimate noise level for a single segment.

$$\begin{aligned} L_{max,j} &= L_{max}(P,d) + \Delta_I(\varphi) - \Lambda(\beta,l) \\ L_{E,j} &= L_E(P,d) + \Delta_V + \Delta_I(\varphi) - \Lambda(\beta,l) + \Delta_F \end{aligned} \tag{3.5}$$

From eq. (3.5), the values of $L_{max}(d,P)$ and $L_E(d,P)$ are obtained directly from the NPD interpolation previously explained. For L_{max} computations, only geometric corrections are made. Instead, the L_E computations also consider corrections due to aircraft velocity and finite segment assumptions. The correction terms are described below.

Δ_V Is the duration correction: As the NPD data is related to a reference speed, this correction factor adjust exposure levels to non-reference speeds.

$\Delta(\varphi)$ Installation effects: describes lateral directivity due to shielding, refraction, and reflection caused by engine and airframe as reported in fig. 2.2.

$\Delta(\beta,l)$ Lateral attenuation: Significant for sound propagation at low angles to the ground. The geometries are the ones reported in fig. 3.6.

Δ_F Finite segment correction: accounts for the finite length of the segment that contributes less noise exposure.

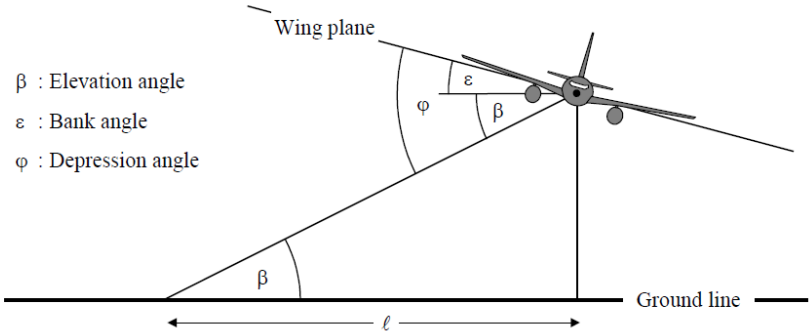

Figure 3.6: Aircraft-observer angles in plane normal to flight track

Source: ECAC [36]

An additional correction is introduced to both terms for landing and take-off roll to account lobed radiation directivity in the rearward arc at higher jet velocities and lower speed aircraft. These corrections Δ_{SOR} are a function of ψ and d_{SOR} which are defined as reported in fig. 3.7

ECAC Doc. 29 gives all the empirical relationships to compute corrected engine power

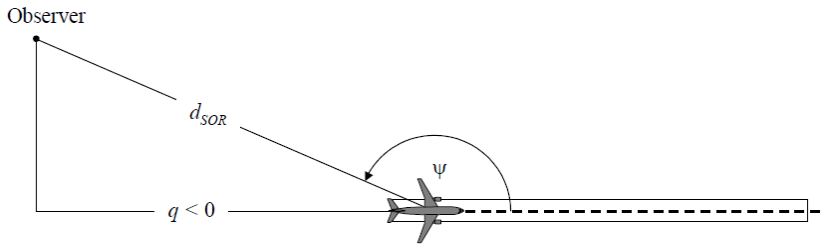

Figure 3.7: Aircraft-observer geometry for estimation of directivity correction

Source: ECAC [36]

and geometric characteristics of each segment. Therefore, L_{max} and L_E for the entire event are computed as eq. (3.6).

$$\begin{aligned} L_{max} &= max(L_{max,j}) \\ L_E &= 10 \cdot \left(\sum^{j} 10^{L_{E,j}/10} \right) \end{aligned} \tag{3.6}$$

3.5. Model implementation

All guidelines provided in the second Volume of ECAC Doc.29 were implemented into a MATLAB program divided into two main modules, the first one for trajectory definition and the second one for noise computations.

The first module receives two general inputs. The first one corresponds to the airport scenario in which the ground track and type of procedure are defined. The second one corresponds to the selected airplane, for which all the data necessary for flight profile definition is obtained from the ANP database. This module defines the trajectory by coupling the ground track and flight profile subroutines.

The second module receives the generated trajectory from the previous module and a defined array of sensitive receivers located on the ground for which noise levels will be computed. This module performs noise computations according to eq. (3.6), then synthesizes and exports results for post-processing analyses such as contour maps generation and comparison of noise impact over different routes.

3.5.1. Model Validation

ECAC Doc. 29 Volume 3 defines a validation procedure to ensure that Volume 2 relationships were correctly implemented. This validation procedure is based on reference cases that provide a set of inputs and expected outputs for use in testing the noise model implementation.

The reference cases consider three hypothetical aircraft configurations on curved(C) and straight(S) notional routes, over arrival(A) and departure(D) procedures as reported in fig. 3.8, which in total corresponds to 12 cases. The aircraft types correspond to:

JETF Turbofan aircraft with engines mounted on the rear fuselage.

JETW Turbofan aircraft with engines mounted under the wings.

PROP Propeller engine aircraft.

Volume 3 suggests three validations steps. For the first two steps, a set of receivers is defined over specific points in the flat earth. Expected SEL values are reported for each receiver and segment. The first step compares the overall SEL due to the entire trajectory. Meanwhile, the second step compares SEL contribution of each segment over specific receivers according to the guideline.

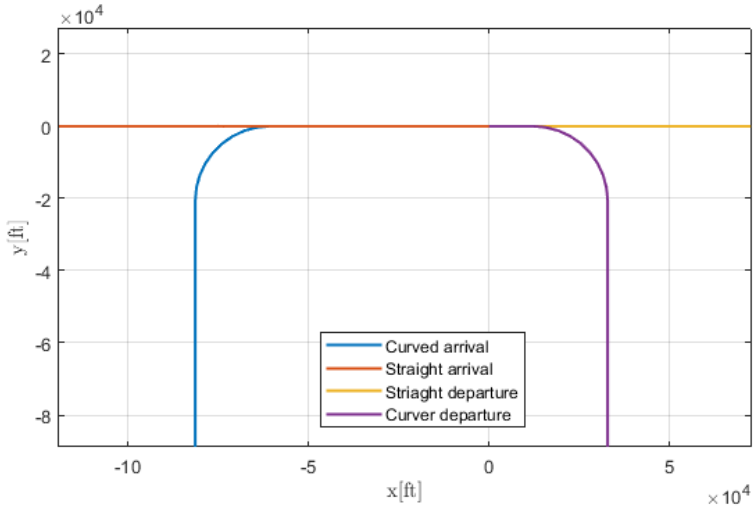

Figure 3.8: Validation scenarios

The third validation step considers noise computation for a dense grid array excluding the runway. Only grid points with noise exposure greater or equal to 80dB are considered to reduce computational effort. For the validation, the root mean square (δ_{RMS}) of the difference between expected and obtained noise levels is computed for the receivers under configuration, see eq. (3.7). Table 3.2 reports all the cases analyzed to validate the model.

$$\delta_{RMS} = \sqrt{\frac{\sum_{i=1}^{N_S} \left(\overline{L_i} - L_i\right)^2}{N_S}} \tag{3.7}$$

	Straight Departure	Curved Departure	Straigth Arrival	Straigth Departure
JETF	0.0030	0.0031	0.0030	0.0028
JETW	0.0030	0.0030	0.0030	0.0033
PROP	0.0030	0.0032	0.0028	0.0028

Table 3.2: Validation results (δ_{RMS}) of ECAC Doc.29 implementation

Volume 3 imposes a δ_{RMS} limit of 0.01dB. As reported in table 3.2, the limit is fully satisfied for all the cases. Therefore, the validation results show the correct implementation of the Volume 2 guidelines.

3.5.2. Radar data synthesis

Additionally, a routine has been implemented for radar data processing. The radar data is accessible from *FllightRadar24* with a silver subscription, and it can be downloaded in *.csv* format for analysis purposes. The data available corresponds to a specific route and time, and it corresponds to:

- Timestamp
- UTC
- Callsign
- Position
- Altitude
- Ground Speed
- Direction/Heading

Python-Pandas have been used for data analysis. As this study focuses on departure procedures, the processing has not been implemented for arrival procedures, but this implementation is straightforward. The routine implemented receives as input the .csv file. It determines the part of the interest mission, i.e., start-of-roll and climb phase for departure.

Depending on the use of the tool, radar data processing can be used for ground track

definition, which is later coupled with flight profiles, or it can be used to define the entire flight path.

4 | Simplified noise modeling

As mentioned in the intro, the main scope of this thesis is to define a simplified noise model that accounts for noise directivity. This model does not need to be highly accurate but must characterize directivity patterns.

The literature presented shows that empirical or semi-empirical approaches can account for noise directivity patterns. The models presented in Chapter 2 follows two different approaches for noise directivity. In the first, directivity is considered directly on the noise computation, as in the FLULA2 model. On the other side, directivity is a correction factor to noise computation like in the AzB model.

The models previously mentioned developed regressions from experimental data available to account for directivity patterns. For this case, experimental data was not available. Due to the extended time and organization needed to perform a measuring campaign to acquire enough data for regression models, it was decided to follow a simulation approach for data acquisition and model definition.

The available implemented ECAC Doc. 29 tool was used for the simulation approach. Although this tool has not been designed for this purpose, it was validated according to the ECAC directives. As ECAC Doc. 29 guidelines do not offer spectral analysis as it is a segmentation-based method. Therefore, the approach followed does not account for spectral decomposition analysis. Instead, it was developed to estimate the overall A-weighted sound pressure level.

FLULA 2 was the reference for the simplified reduced model definition due to its simplicity and the fact that the final estimation corresponds to the OASPL. Since it was impossible to perform spectral analysis, the regression was performed over the noise computations from the implemented tool.

Then, L_{max} measurements were the metric used for the data acquisition. This metric was used because it depends on a specific segment and geometry between the aircraft and receiver position. Instead, SEL was not considered because it corresponds to an integral metric that depends on the previous and following segment.

Up to now, the NOICE model is only focused on departure procedures. Then, for simplicity, the study focused on departure procedures considering an Airbus 320 model that corresponds to a wide-body commercial aircraft commonly operated in European airports.

4.1. First approach

The first approach tried considered an airport scenario with a defined ground track and a default procedure from the ANP database. The data acquisition defined a dense grid of ground receivers following the same principles used in the model validation.

In this case, the data acquisition measured L_{max} for each receiver on the ground and each segment with the respective geometry of interest, like the slant distance and radiation angle. This approach was used to assimilate noise time history level, which would be measured by a noise monitoring terminal.

The scenario definition is presented in fig. 4.1, in which it is possible to identify the flight path and the grid of sensitive on-ground receivers.

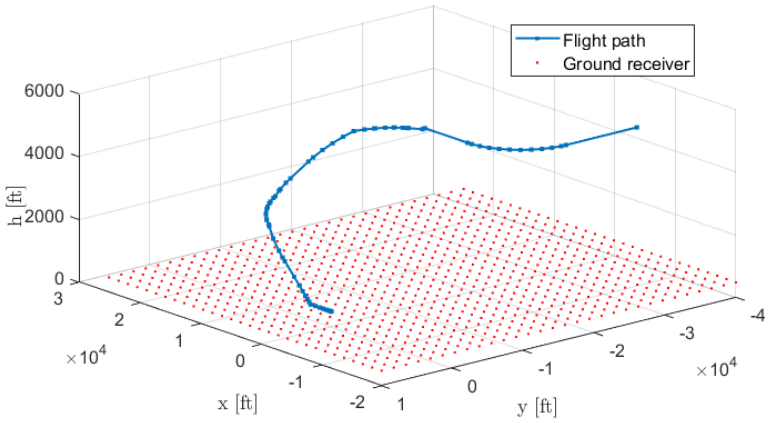

Figure 4.1: Simulation approach flight path scenario with ground receivers

A simplified version of FLULA 2 reported in eq. (4.1) was used. It corresponds to simplification from eq. (2.2) and eq. (2.3) presented in chapter 2. The original equation is based on spectral analysis reconstruction to a referende distance, so it looks for 32 coefficients for a defined distance R. Instead, eq. (4.1) does not account for sound level reconstruction and finds the coefficients directly from the L_{max} measurements from the simulations.

$$L_{OA}(R,\theta) = \sum_{k=0}^{7} A_k(R) cos(\theta)^k$$
$$A_k(R) = H_{k1} \cdot 20\, log(R) + H_{k2} + H_{k3} \cdot R + H_{k4} \cdot R^2 \tag{4.1}$$

With the simulation data, MATLAB's Curve Fitting Tool was used to find the 32 coefficients of the model according to eq. (4.1). The Fitting Tool used the nonlinear least-squares method for finding coefficients and receives as inputs the slant distance, radiation angles, and L_{max}, to find the regression model coefficients.

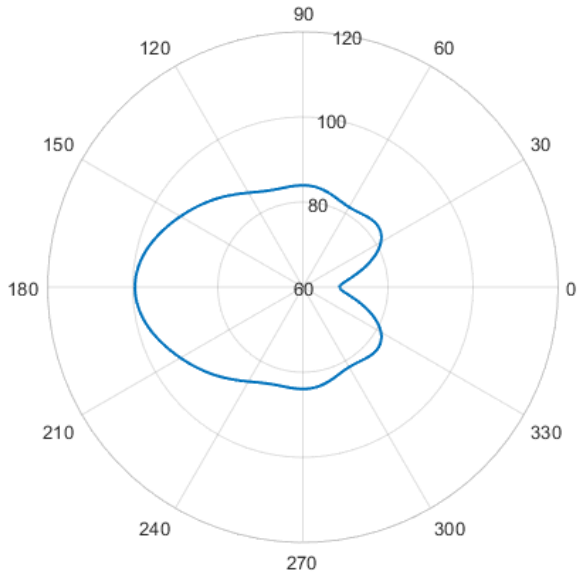

Figure 4.2: 1^{st} approach A320 Sound pressure level [dB] at 1000ft

Figure 4.2 reports the result of the fitting analysis for the simulated data where 0° corresponds to aircraft nose; therefore, 180° corresponds to aircraft tail. The noise directivity pattern is symmetric to the longitudinal aircraft axis.

Specifically, it reports the noise level at a distance equal to 1000ft or 305m. This distance is chosen for initial comparison because FLULA 2 model considers this distance for the normalization of its measurements and AzB reports noise pressure level at 1000ft, as shown in fig. 4.3.

Therefore, it is possible to visually compare the shape of the directivity patterns with the references from the literature. Figure 4.3b from the FLULA2 model is the result of noise regression for an MD11, a tri-jet wide-body aircraft. Figure 4.3a from the AzB model shows the directivity correction for the aircraft class in which an A320 is part.

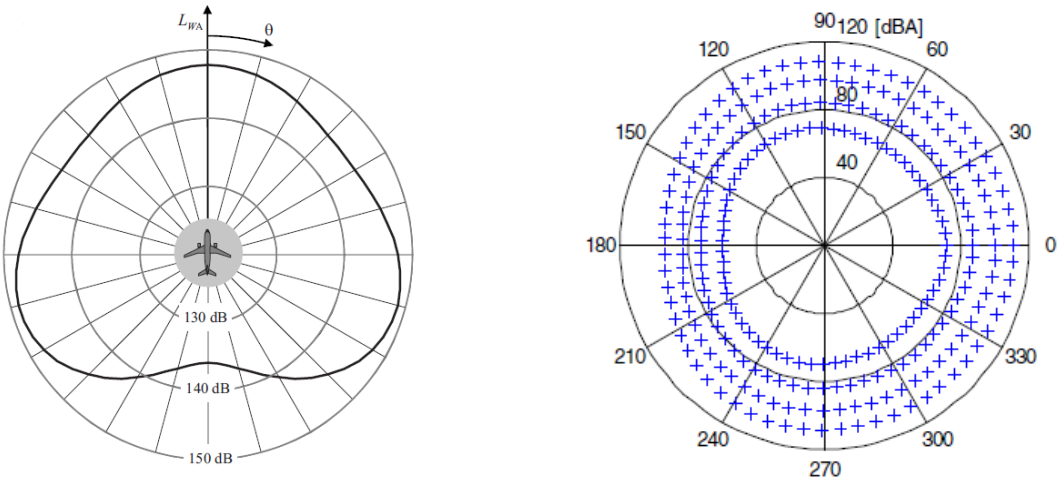

(a) AzB model results

(b) FLULA 2 model results

Figure 4.3: Directivity patters from the literature.

Despite the non-accurate analysis performed, comparing the obtained result with the available directivity models, a considerable difference from a visual point of view was evidenced.

This last behavior can be explained by fig. 4.4, which visually reports the fitting results. The blue dots represent the simulation data, and the surface represents the fitting function according to the eq. (4.1). There is a considerable noise level dispersion, especially at low radiation angles where data points with lower noise levels than the fit function. This behaviour is contrary to fig. 4.3, which shows higher noise levels in the nose direction instead of the tail direction.

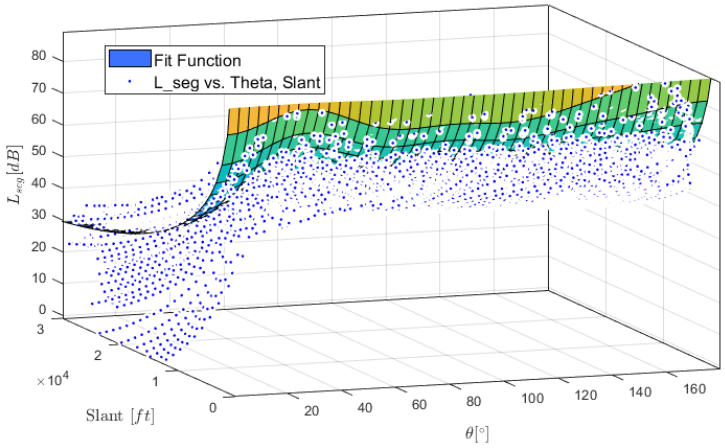

Figure 4.4: 1^{st} approach function fitting results

From the previously exposed results, the simulation approach that tried to follow a flyover event's real measurement does not give expected results. From a visual point of view, it does not match the expected shape from the literature. This is mainly due to the considerable dispersion at certain angles due to the intrinsic singularities of the procedure itself.

As previously mentioned, this guideline was not developed for such analyzes. As reported in fig. 4.4, the dispersion points correspond to points at low angles and generally low noise levels, so it could be assumed that these points eventually will not be the location where the L_{max} is registered for the event. Therefore, it is impossible to rely on the obtained results.

The Fitting Tool gave as output the regression performance. The R-square value corresponds to 0.87. Therefore, this measurement defines a metric for performance comparison with following approaches.

4.2. Second Approach

Another approach was tried to overcome the problems encountered with the previous method. This second approach did not try to obtain an equivalent of the time history level of an event, but instead, it was based on the L_{max} over the entire flight path.

Consequently, this approach computed the L_{max} over each receiver for the entire trajectory instead of computing it for every segment, i.e., it follows the eq. (3.6). This approach was followed to reduce the inconsistencies evidenced in the previous analyses.

This method gave fewer data points, so a denser receiver array and multiple scenarios were defined and analyzed to obtain a more extensive data frame for analysis. Also, for simulation improvements, the segment distance was reduced. Figure 4.5 reports two of the multiple scenarios performed, one with a straight departure and the other with a procedural departure based on Milano Malpensa SID.

For the fitting routine, the same modified eq. (4.1) was considered. After extensive simulations for data acquisition, the results are reported in fig. 4.6, and show the OASPL as a function of the direction at a slant distance of 1000ft. In this case, the shape of the figure is similar to the bibliography. Also, this approach presents better fitting performance, where the R-square went from 87% to 99.6%.

Figure 4.7 shows the OASPL varying the propagation distances. It is evident that as the slant distance increases, the directionality pattern begins to deform and show shapes

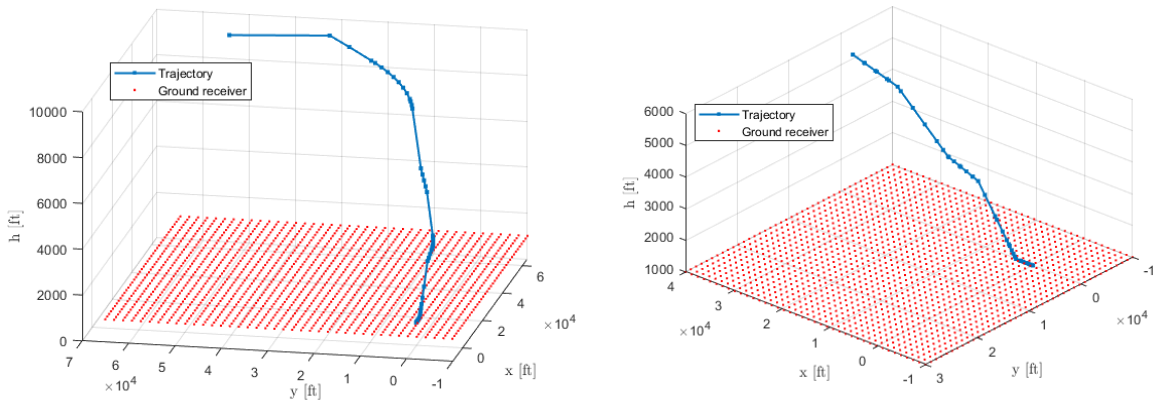

(a) SID departure simulation

(b) Straight departure simulation

Figure 4.5: Departing simulation scenarios

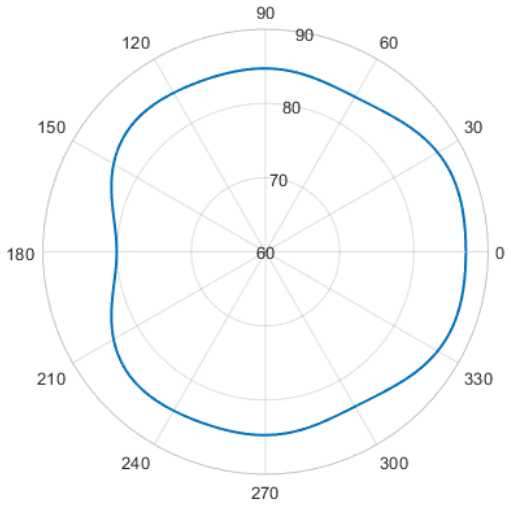

Figure 4.6: 2^{nt} approach A320 Sound pressure level [dB] at 1000ft

highly non-omnidirectional (i.e., a circular shape). From the figure, up to a certain slant distance, the directivity patterns seem to converge onto a circular shape, corresponding to the expected behavior as the turbofan aircraft's directivity is approximately omnidirectional [41]. However, as the slant distance increases, the directivity patterns deform to non-circular shapes.

Different factors can explain this last behavior. The first one corresponds, as mentioned before, to the lack of data over the entire domain to study. Figure 4.8 shows the combination of slant distance and θ for simulation data. This last figure shows areas for which there is no data from the simulation, even performing different simulation scenarios. For slant distances larger than 15000ft, there is no data points for angles between 110° to 180°

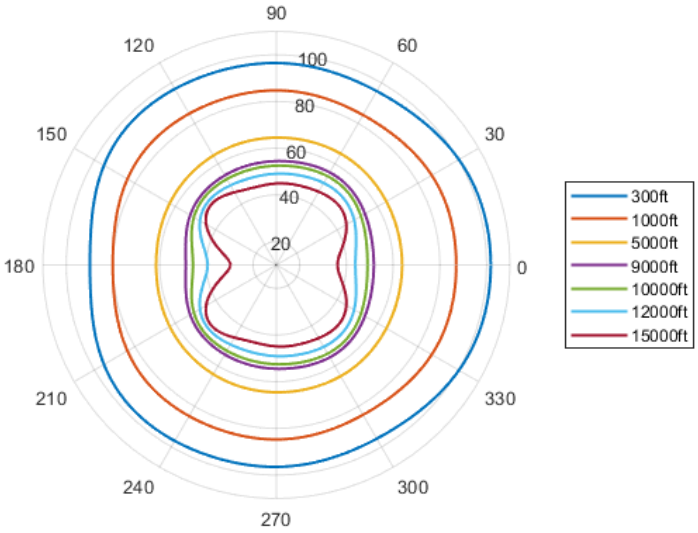

Figure 4.7: 2^{nd} approach A320 sound pressure level [dB] at different distances

and, as the slant distance increases, there is data only for the range of θ between 60° and 110°.

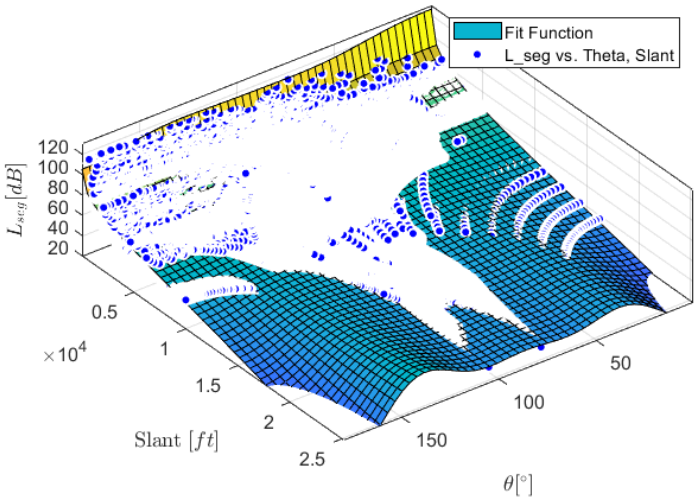

Figure 4.8: 2^{nd} approach function fitting results

Despite R-square value is equal to 99.6%, this last value is obtained comparing the available data with the resulted function. Therefore, for the zones where there is no data, the function is not reliable even for the R-square value obtained.

A second explanation could be due to the non-robustness of the approach due to the simplifications considered to the regression function implementation as it measures the

OASPL instead of performing spectral analysis, where attenuation effects are not being considered.

Anyhow, this behaviour takes place at more considerable slant distances for which the noise level could be insignificant for the optimization tool. In fact, from fig. 4.7, it is evidenced that for 10000ft, the max SPL is equal to 50dB, comparable with a quiet urban zone.

Then, two approaches for the implementation were proposed to the optimization tool developers.

The first one was to neglect all the noise levels with a slant distance greater than a defined threshold. This approach can reduce the computational effort, but it can introduce problems to the optimization routine. Precisely, due to the zero-noise, zero-cost paths, for which the tool would follow these zones that can considerably increase route length and non-convergence.

The second option was to define a constant noise level for larger slant distances. With this approach, a more realistic implementation is considered defining a noise level compared to a quiet street or rural zone. With this consideration, all the sensitive receivers weights for the optimization.

4.3. Implementation

The final step in the development of the simplified model was its implementation. In the previous section it was seen that for greater distances, the model presented certain irregularities. In this section is presented the analysis developed to obtain a model with engineering application, which was implemented as a function in Python, that corresponds to the programming language used by the NOICE program.

To implement the model for the optimization tool, a comparison of the omnidirectional trend of the obtained function from the regression was performed. Figure 4.9 shows the difference between the max and min SPL varying the slant distance. Where it is shown that the shape tends to be an omni-directional one(i.e., circular shape), up to 4000ft, but after that distance, the max and min difference starts to increase,(i.e., non-omnidirectionally) as showed in fig. 4.7.

For the implementation, the idea was to consider a function that tends to an omnidirectional behavior as the slant distance increases. Therefore, it considered the inverse square law for the sound pressure level as reported in the eq. (4.2), where the SPL at a

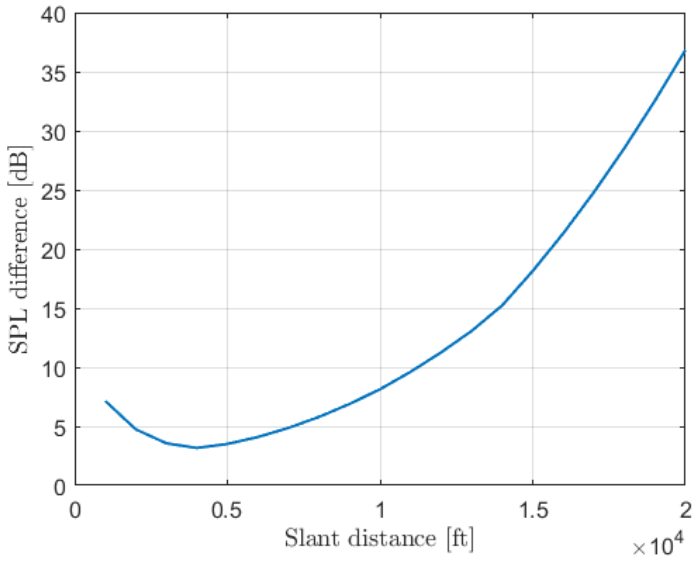

Figure 4.9: Maximum and minimum SPL difference varying slant distance

distance r_2 from the source can be computed knowing the SPL and distance at point 1. For this case, point 1 was selected at 4000ft, corresponding to the "most omnidirectional" directivity patterns. This last equation only accounts for spreading effects such as the current model used. The result of this consideration is reported in fig. 4.10.

$$L_{p2} = L_{p1} + 20 \log \left(\frac{r_1}{r_2} \right) \tag{4.2}$$

Figure 4.10 presents a considerable difference in noise level comparing with the simplified model from the regression as the slant distance increases. The SPL does not decrease at the same rate as seen in fig. 4.7. Instead, the "shape" of directivity remains the same as the reference ot 4000ft.

Figure 4.11 shows the difference up to 20000ft for different directions of the SPL obtained between the regression and the estimated level from eq. (4.2) reported in fig. 4.10, considering as reference the SPL at 1000ft.

Hence, eq. (4.2) generally overestimates the SPL for all the directions. This can be explained due to the simplicity of the relationships that only account for geometric spreading (inverse square law) but not for attenuation effects such as those exposed in eq. (2.1) .

From literature, the relationship of eq. (4.3) presents a more accurate estimate of the SPL with correction factors due to atmospheric attenuation(α_i, $\alpha_{0,i}$) and ground reflections Δ_i. This last equation is frequency-dependent. Therefore, spectral analysis should be

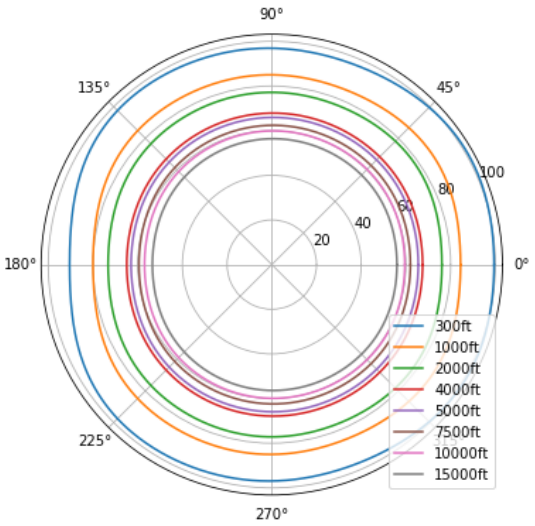

Figure 4.10: A320 sound pressure level with inverse square law after 4000ft

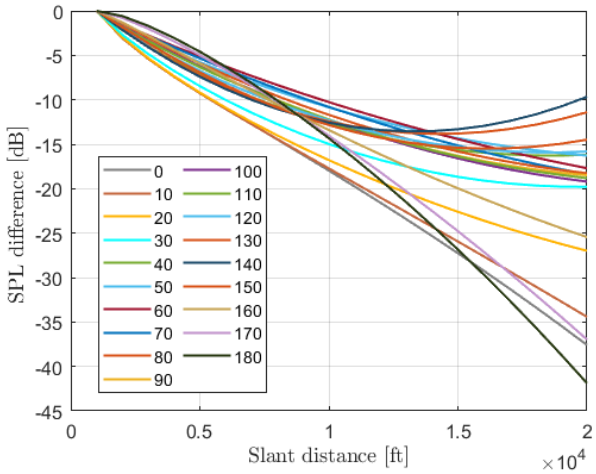

Figure 4.11: Comparison of regression model vs inverse square law with reference at 1000ft

performed for accurate analysis.

$$L_{p2,i} = L_{p1,i} + 20\log\left(\frac{r_1}{r_2}\right) + \alpha_i \cdot r_1 + \alpha_{0,i} \cdot r_2 + \Delta_i \tag{4.3}$$

Anyhow, a regression was performed to find a function that describes the non-considered attenuation effects of the simple inverse square law. To implement this regression it was considered the radiation angles for which there is consistent data over the different slant distances derived from Figure 4.8, between 60° and 110°. The regression result is reported in eq. (4.4) and the fits is evidenced in fig. 4.12.

$$f(R) = 3.6 \cdot 10^{-8} R^2 + 0.00161R + 1.468 \tag{4.4}$$

With this regression, it was defined a piecewise function. This function uses the regression according to eq. (4.1) up to 4000ft of slant distance . From 4000ft it considers the directivity pattern of eq. (4.1) at 4000ft as reference measurement and estimates the SPL using the inverse square law of eq. (4.2) with a correction term of eq. (4.4) for the non modelled attenuation effects.

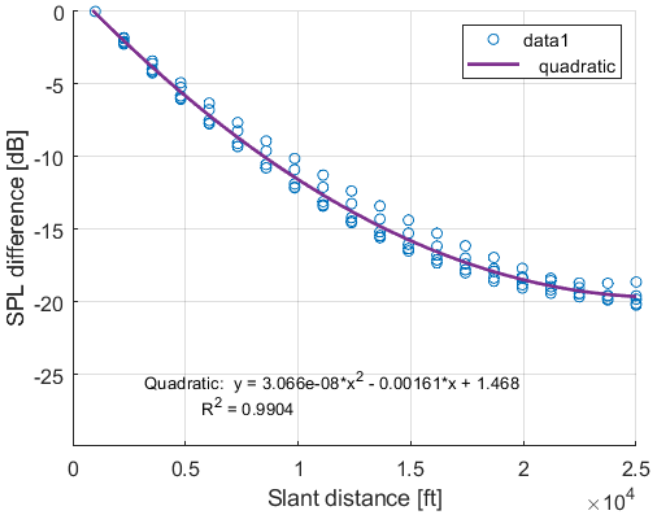

Figure 4.12: Regression for non modelled attenuation effects

Finally, it was determined the distance for which the minimum SPL is equal to 40dB, which is comparable to a quiet rural area(see fig. 1.5). Then, for larger slant distances, the SPL is set at 40dB to model what would be rural locations for which the contribution of the aircraft motion would not modify the SPL of the ambient itself. The final piecewise equation is presented in eq. (4.5) and the simplified model is shown in fig. 4.13.

$$L(R,\theta) = \begin{cases} \sum_{k=0}^{7} A_k(R) cos(\theta)^k & [dB] \quad R \leq 4000 \\ \sum_{k=0}^{7} A_k(4000) cos(\theta)^k + 20 \log\left(\frac{4000}{R}\right) + f(R) & [dB] \quad 4000 < R \leq 13000 \\ 40 & [dB] \quad R > 13000 \end{cases} \tag{4.5}$$

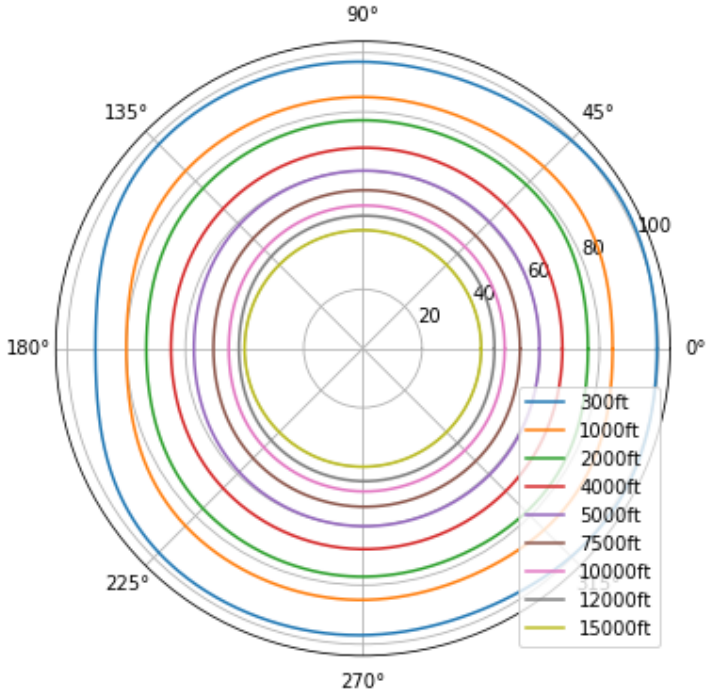

Figure 4.13: Final A320 sound pressure level model for algorithm implementation

4.4. Computing time comparison

For quantifying the computational effort difference of the simplified noise model with the spherical spreading, it was measured how long it took to call both functions a certain number of times. The results are reported in table 4.1, for which the functions were called between 10,000 and 10,000,000 times with random values for slant distances and radiation angles. Therefore, the SPL estimated with the simplified noise level is close to 57 times slower than the initial spherical spreading estimation. This is explained mainly for the number of calculations compared with the spherical spreading calculations.

The number of times the SPL is estimated in NOICE depends on multiple factors, which are defined in the program set-up such as:

- Number of sensible receivers
- Segment length
- Ramification rate
- Distance between starting and goal point

These items are not discussed in detail but depending on the configuration, the times which the functions are called is between 10^5 to 10^7. Therefore, the NOICE tool would

takes extra 200s to find the optimum solution in the worst case.

Function calling times	Spherical spreading [s]	Simplified model [s]	Ratio [-]
10 000	0.004	0.205	51.25
50 000	0.015	1.099	73.27
100 000	0.034	2.08	61.18
500 000	0.175	9.819	56.11
1 000 000	0.349	19.629	56.24
5 000 000	1.848	98.2	53.14
10 000 000	3.637	195.93	53.87

Table 4.1: Models computing times comparison

5 | Application studies

This chapter aims to quantify and assess the NOICE model results before and after utilizing the simplified noise model that accounts for directivity patterns. The study was focused on Milano Malpensa Airport, and the results of the NOICE model was compared with noise-abatement procedures currently defined at the airport.

Consequently, the study cases determined if the simplified noise model accounts for considerable noise exposure reduction over the communities close to the airport area, compared with the spherical spreading modelling previously implemented.

5.1. Scenario definition

The scenario selected for the study cases corresponds to Milano Malpensa Airport (IATA: MXP, ICAO: LIMC) that features two parallel runways (35L/17R, 35R/17L), see fig. 5.1. The airport is in the municipalities of Somma Lombardo and Ferno, in the province of Varese, in northern Italy. It is the second Italian airport for passenger traffic [42].

SEA Group is the current airport operator, up to now, SEA has carried out an acoustic mapping of the airport as required by Legislative Decree 194 of 2005 [43]. This mapping analysis has been performed using the INM tool provided by FAA. On this analysis, the municipalities of Somma Lombardo and Lonate Pozzolo are the ones most exposed to aircraft noise. Therefore, the SEA group has implemented anti-noise measures in compliance with the ICAO Balance approach, such as [44]:

- Limitation of aircraft type according to ICAO annex 16 chapter 3
- Implementation of noise abatement procedure, especially new departure procedure from runway 35R/17L
- Utilization of precision P-RNAV routes for maximum track of the selected route
- Traffic distribution between both runways
- Optimized initial climb and approach profiles

- Operating restrictions at night for which

The study was focused on the SID departure from the runway 35R, specifically, the DOGUB5T, which can be seen in fig. 5.2. Eventually, for comparison purposes two additional study cases were defined based on departure procedures from runway 17R.

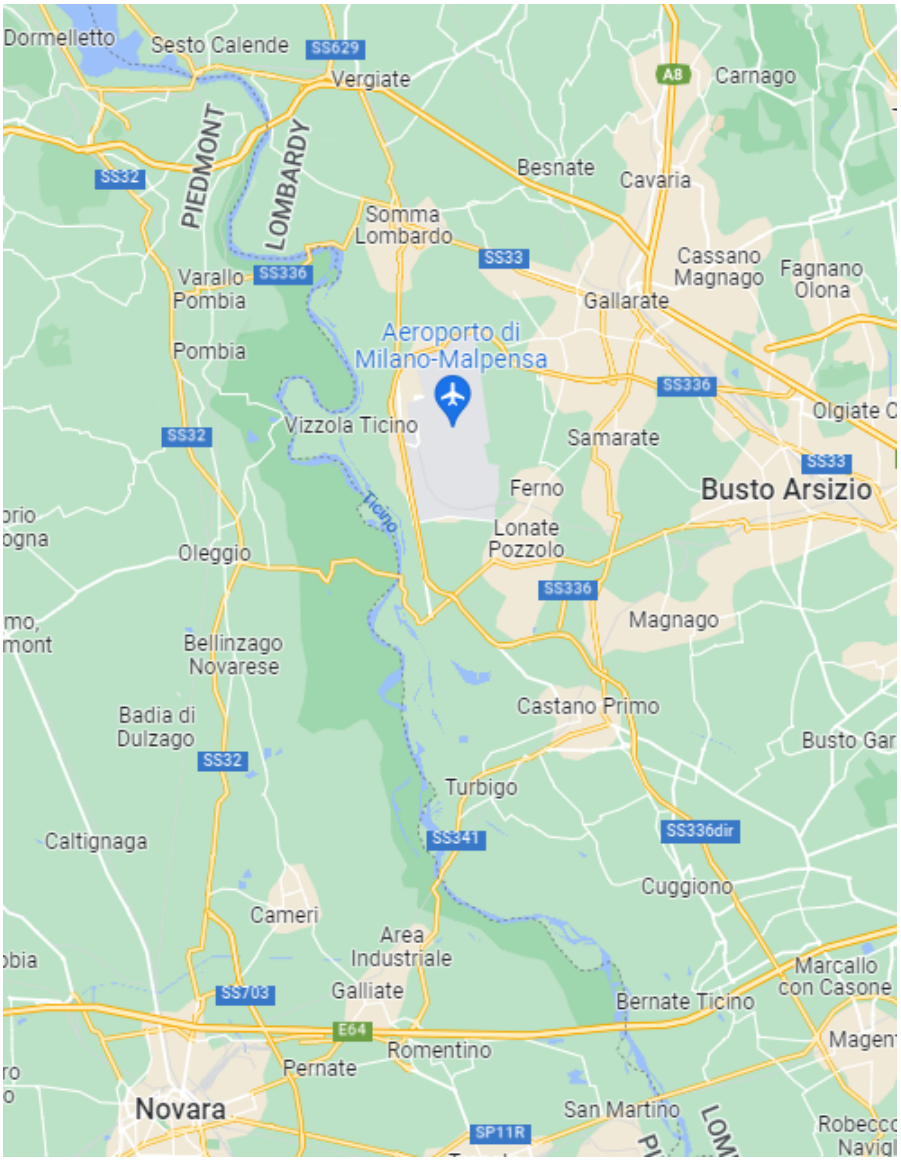

Figure 5.1: Milano Malpensa Airport area

Source: Google Maps

In addition to Somma Lombardo and Lonatte Pozzolo, in the vicinity of the airport, several municipalities are affected by noise due to the airport's location. Therefore, the noise impact study considered all these locations corresponding to the airport area reported in table 5.1.

Location	Population
Lonate Pozzolo	11483
Nosate	640
Castano Primo	10980
Turbigo	7092
Somma Lobardo	17785
Varallo Pombia	4847
Pombia	2131
Molinara	1484
Vergiate	8641
Arsago Seprio	4806
Robecchetto con Induno	4775
Sesto Calende	11055
Borgo Ticino	5159
Cuggiono	8194
Inveruno	8525
Varese	79350
Novara	102225

Table 5.1: Airport area municipalities

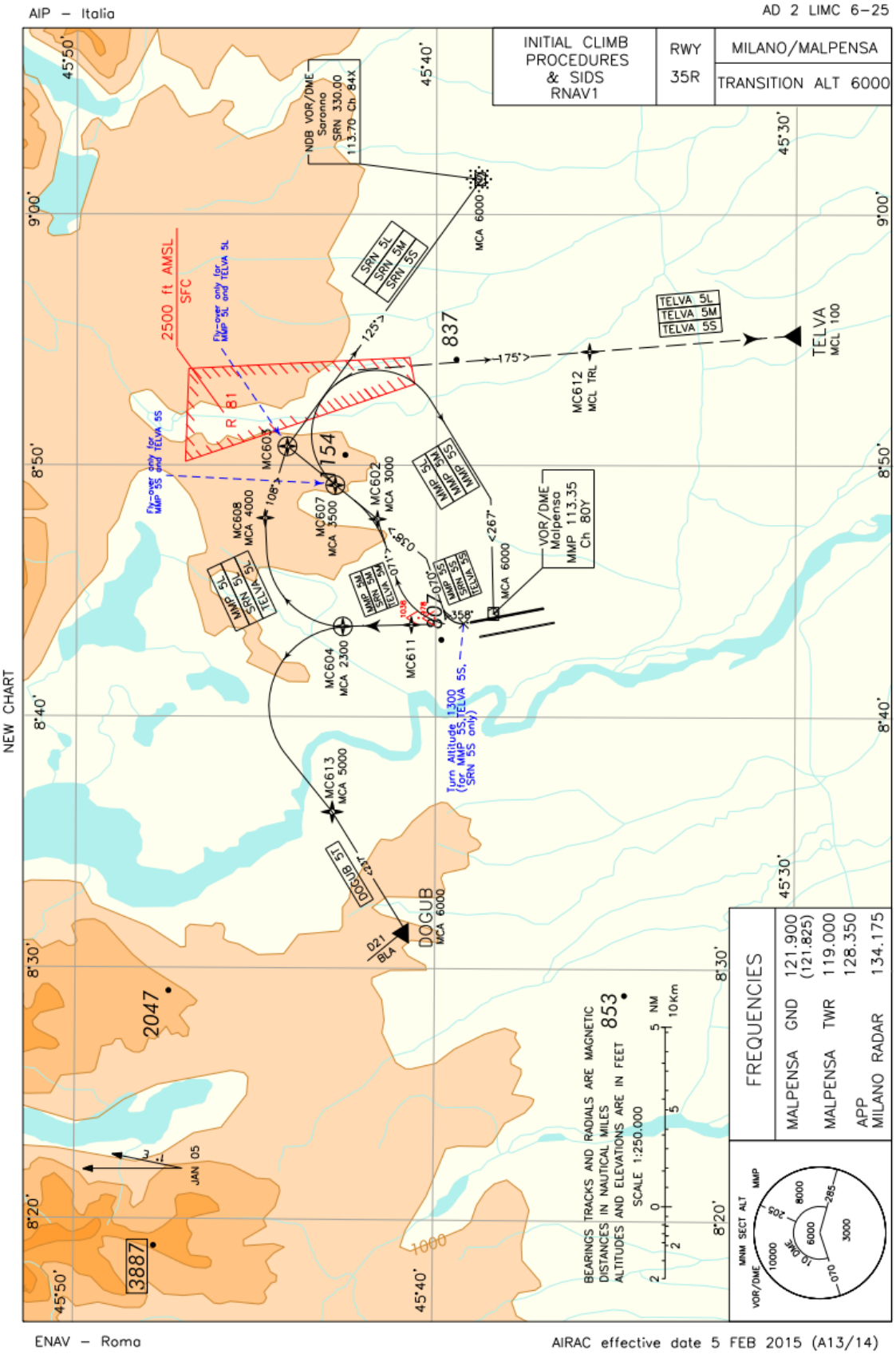

Figure 5.2: Milano Malpensa runway 35R SID

5.2. Methodology

The study compared the optimal routes from the NOICE optimization tool with the noise abatement procedure currently defined and reported in fig. 5.2.

For the current noise abatement procedures SID, the ground track was defined using available radar data from FlightRadar24. As previously mentioned, the available flight radar data gives aircraft position over time in geographic coordinates.

Python was used to process these data and convert the segments from geographic coordinates to Cartesian ones, with origin at the break-release and x-axis aligned with the runway.

NOICE results are also reported in geographic coordinates. Therefore, the same Python routine converted the segments to Cartesian coordinates.

As NOICE outputs correspond to ground track segments, only the ground track from FlightRadar24 data was used to compare them correctly. In this way, all the cases had the same flight profile defined from the standard procedures present in the ANP database, that corresponds to the same flight profiles used to obtain the simplified model of chapter 4.

In this case, the measure to compare the performance of the routes was the sound exposure level (SEL) because, as its name, it indicates the exposure to the noisiness of the event. Thus, the SEL was calculated on all the sensitive receivers indicated in table 5.1. Cumulative metrics were not computed because they depend on single even metrics and analyze overall airport scenarios, including multiple runways operation, aircraft and schedules. For comparison purposes, the analyses accounted only for the receivers with SEL higher than 50dB.

The study also compared the differences between the spherical spreading model and the simplified one. In the following sections, NOICE V1 will refer to the optimum solutions found with the spherical spreading model. Instead, NOICE V2 will refer to the simplified noise model's optimum solutions previously defined.

5.3. Real scenario analysis

Figure 5.3 represents the flight path synthesis from ground track definition based on flight VY6329 from LIMC to El Prat Airport Barcelona (LEBL) departed at 12:30 on March 15, 2022. This flight took off from runway 35R towards the northeast and finally went west to Barcelona.

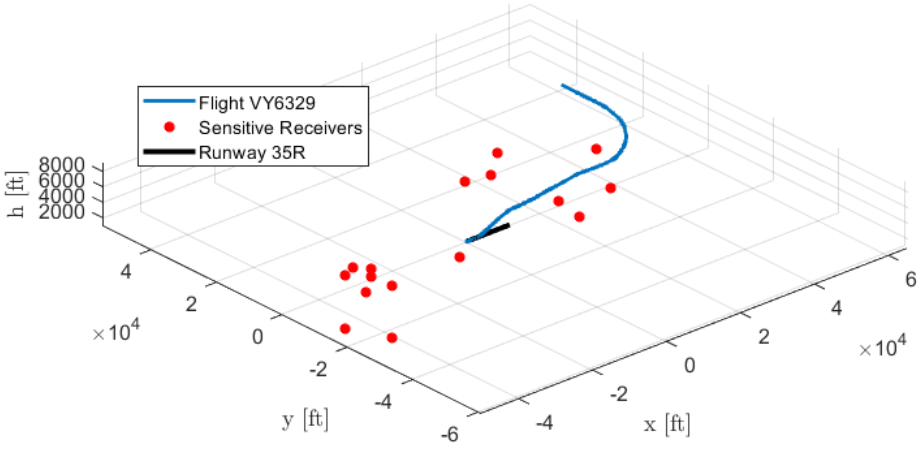

Figure 5.3: Flight VY6329 DOGUB5T departure procedure

Table 5.2 presents the SEL over the sensitive receivers with more than 50dB. Almost all the sensitive receivers are located north of the airport, in the direction of the departure route.

Location	SEL [dB]
Borgo Ticino	67.09
Varallo Pombia	61.44
Somma Lombardo	77.59
Lonate Pozzolo	67.95
Pombia	59.71
Arsago Seprio	75.45
Sesto Calende	72.12
Vergiate	77.07
Molinara	52.10
Nosate	52.33

Table 5.2: Flight VY6329 SEL over sensitive receivers

Table 5.2 shows that the communities with higher noise exposure levels correspond to Somma Lombardo, Arsago Seprio, Vergiate, and Sesto Calende with SEL higher than 70dB. These municipalities are located close to the projected ground track of the departure, as shown in fig. 5.4.

As observed in fig. 5.4, the SEL decreases for the municipalities that are further from the airport even though they are closer to the projection of the trajectory. As the aircraft moves away from the airport, it continuously climbs, so the distance between the aircraft and the receiver is greater, and therefore, the SEL is lower.

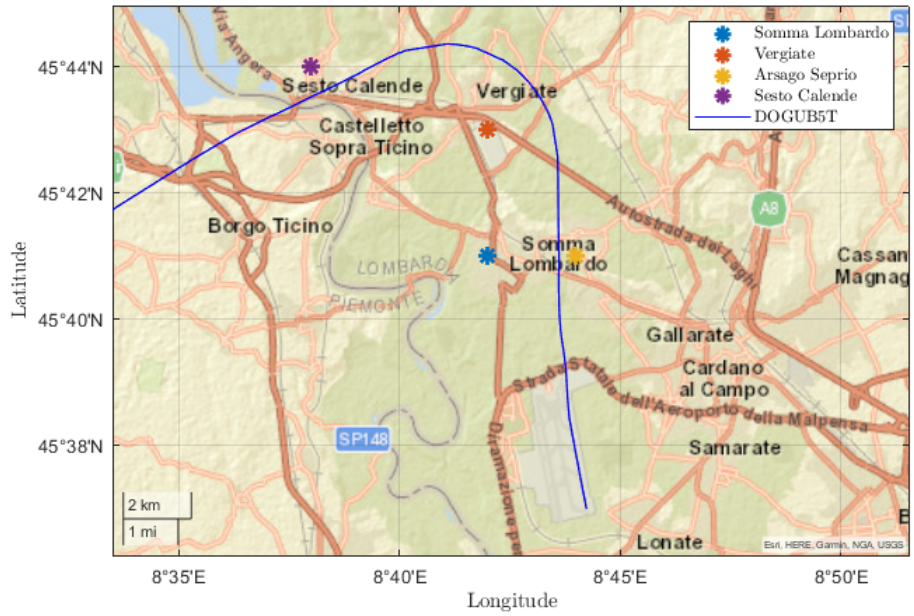

Figure 5.4: Flight VY6329 departure ground track projection

With these reference values, the next step was to compute the SEL over the sensitive receivers for the generated ground trajectories of the NOICE tool.

5.4. NOICE V1

An evaluation of optimum results of the first version of NOICE was performed to analyze the current model and eventually compare it with the improved one, which uses the new aircraft noise model that accounts for directivity. This version was the one that accounts for aircraft noise as a single source with omnidirectional propagation modeled with the ISL.

For this case, the start location is 45.6174° latitude and 8.7370° longitude, with an azimuth of 348°, aligned with runway 35R. The start location corresponds to the brake-release point of runway 35R. The goal location is 45.6808° latitude and 8.5254° longitude, with an azimuth of 237°, which corresponds to the end of the route from the flight VY6329.

NOICE output corresponds to a set of waypoints from which the ground track segments are defined. The first segment length is 1000m, which assimilates the take-off distance. After that, the length of each segment corresponds to 2500m, for which turns can be performed to follow the optimal route.

Although this take-off distance did not correspond with the aircraft studied, it was studied to evaluate the sensitivity of the optimization tool to the initial segment length. Then, another case was studied to account for a compliance case. This last result has a 2km initial length as a constraint for the optimization tool. Therefore, three cases were defined for the analysis:

Case 1 Current SID from runway 35R

Case 2 Runway 35R departure with 1km of take-off distance

Case 3 Runway 35R departure with 2km of take-off distance

Location	Case 1 SEL [dB]	Case 2 SEL [dB]	Case 3 SEL [dB]
Somma Lombardo	77.59	65.61	69.33
Vergiate	77.07	60.46	57.91
Arsago Seprio	75.45	73.89	61.76
Sesto Calende	72.12	64.61	58.86
Lonate Pozzolo	67.95	68.16	67.36
Borgo Ticino	67.09	66.21	75.68
Varallo Pombia	61.44	59.07	72.32
Pombia	59.71	57.88	65.80
Nosate	52.33	51.71	50.62
Molinara	52.10	49.78	50.67
Average	**66.28**	**61.74**	**63.03**
Log-Average	**72.40**	**66.49**	**68.75**

Table 5.3: SEL case comparison

Table 5.3 reports the result of the SEL over the sensitive receivers the cases previously defined. For some municipalities, the SEL decreases with the new optimal routes; meanwhile, for others, the SEL increases, but in general, the log-average SEL decreases with both new optimal routes.

Table 5.4 summarizes the difference at each receiver between case 1 and the rest. For case 2, the SEL decreases for all the sensitive receivers; meanwhile, for the case 3 route, the SEL increases for certain municipalities, where the most affected municipalities correspond to Borgo Ticino and Varallo Pombia.

The traveled distance is an aspect to consider for the optimization routes because, as stated by the ICAO, the balanced approach is focused on achieving maximum environmental benefit most cost-effectively. Table 5.5 shows the ground-track distance from the brake release point to the final point covered by each route. Case 3 travels the shortest

Location	ΔSEL Case 1-2 [dB]	ΔSEL Case 1-3 [dB]
Somma Lobardo	-11.98	-8.25
Vergiate	-16.61	-19.16
Arsago Seprio	-1.56	-13.68
Sesto Calende	-7.51	-13.26
Lonate Pozzolo	0.21	-0.59
Borgo Ticino	-0.88	8.58
Varallo Pombia	-2.37	10.88
Pombia	-1.84	6.09
Nosate	-0.61	-1.71
Molinara	-2.32	-1.43

Table 5.4: SEL difference comparison with ISL noise model

distance for the cases studied, while case 2 travels the largest distance, even more than the base case.

Case	Ground distance covered [km]
1	33.23
2	49.32
3	21.55

Table 5.5: Comparison of ground distance covered

Figure 5.5 shows the ground track followed for each departure route, where it is evidenced that the route considering 2km of take-off distance is the shortest one. From the results, it is possible to see a considerable difference in the routes varying the take-off distance. Despite this analysis only considered an A320 aircraft, the final scope of this optimization tool would be to define optimal routes for different aircraft and, therefore, different take-off distances.

Case 3 seems to be the optimal solution even compared with the current noise abatement departure routes. Anyhow, a further analysis over the ground trajectory flown was performed.

Figure 5.6 shows a zoom on the routes in the airport area, where it is possible to evidence a potential implementation problem. The yellow route corresponding to case 3 crosses the eventual runway 35L departing or arrival route, an action that may jeopardize the safety of the procedure and the flight. Therefore, particular constraints should be implemented on the optimization tool to prevent these results. These constraints will depend on the

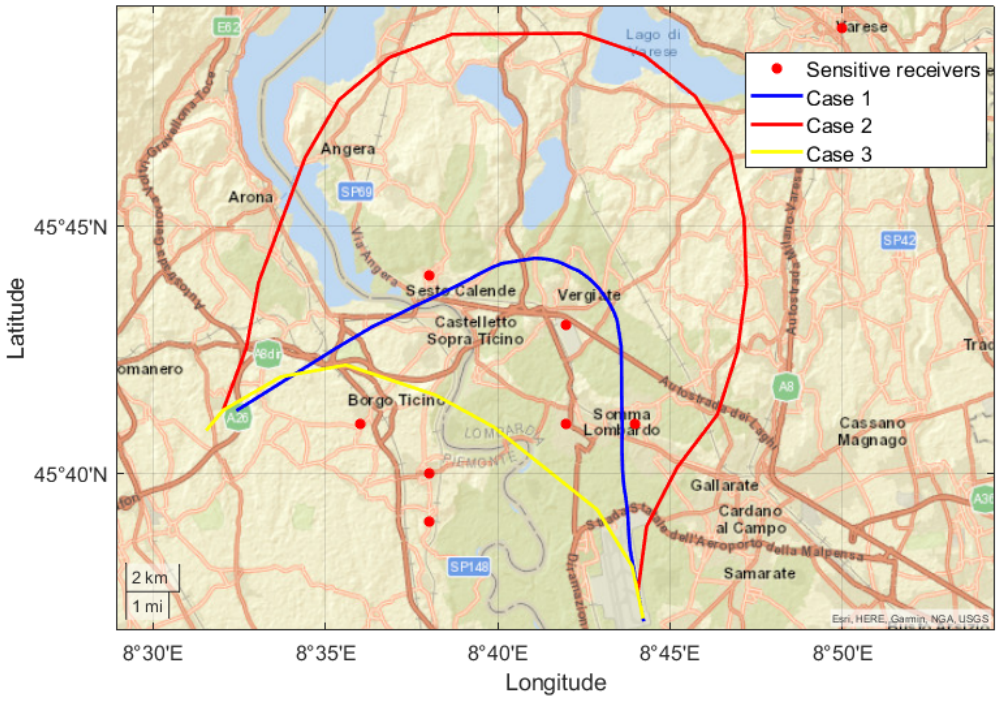

Figure 5.5: Comparison of ground track projection between current SID and optimal solutions

scenario to study, and a recursive analysis between optimization tool and validation could lead to a final optimal route.

NOICE V1 has shown general improvements in the SEL over communities close to the airport. From this analysis, several considerations are made. The first one corresponds to validating the obtained results in the real scenario to identify possible implementation problems. The second is the trade-off between SEL reduction and increased traveled distance, which could derive into general non-cost-effective procedures.

These analyses also give feedback to the optimization tool implementation that could be helpful to improve the overall robustness of the NOICE model, even when all the results of the tool should be validated under the real scenarios.

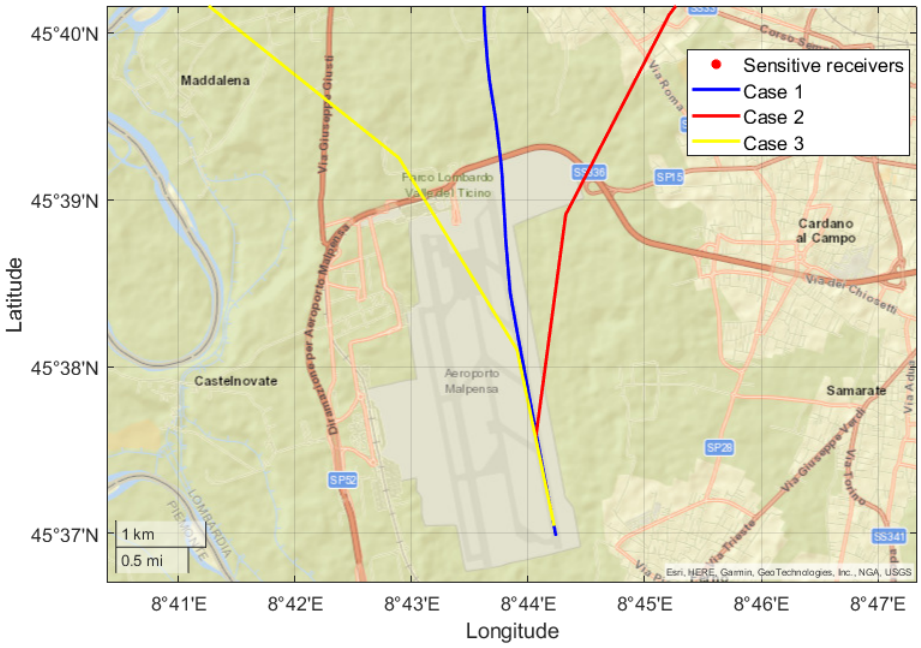

Figure 5.6: Airport zone ground track projection comparison

5.5. NOICE V2

After analyzing the study cases comparing the current noise abatement departure and the optimized routes from the NOICE tool, the program underwent modifications to increase its robustness.

The noise modeling modification comprises the utilization of the defined simplified noise model obtained through simulation, and the addition of the altitude dimension considering a constant rate of climb. Then, it was possible to compute the slant distance and the radiation angles to use the simplified noise model.

The case study below compared the results of the optimal routes after the modifications. The objective of the comparison was to determine and quantify the difference of the optimal route due to changes in the noise model and thus determine if it is beneficial to consider this model or is enough to consider the previous model based on the inverse square law. Therefore, the purpose is not to evaluate the optimal route's behavior or feasibility under a real scenario since the NOICE tool will continue its development. Hence, two cases were defined to analyze.

Case 4 Runway 35R departure with 2km length of initial segment distance with the new simplified noise model

Case 5 Runway 35R departure with 5km length of segment with the new simplified noise model

Case 4 was selected to directly compare the SEL of the new optimal solution under the same scenario characteristics of Case 3, 2km length of the first segment. Additionally, Case 5 considered a 5km length for the initial segment to evaluate an eventual constraint that does not permit a left turn just after take-off.

The results of these new cases are reported in table 5.6, in which, again, Somma Lombardo municipality is the one with the higher noise exposure level for both cases.

Location	Case 4 SEL [dB]	Case 5 SEL[dB]
Somma Lobardo	75.07	79.15
Vergiate	63.97	66.23
Arsago Seprio	66.37	70.07
Sesto Calende	67.01	67.77
Lonate Pozzolo	67.63	67.88
Borgo Ticino	68.14	67.45
Varallo Pombia	66.16	64.29
Pombia	62.95	60.97
Nosate	51.47	52.06
Molinara	51.38	52.05

Table 5.6: SEL case comparison for optimum routes with the simplified noise model

Table 5.7 compares the results of these new cases concerning the current SID of Case 1. Case 4 reports a minor decrease in the SEL for Somma Lombardo, Vergiate, and Arsago Seprio municipalities than case 3, but the increase of SEL for the Borgo Ticino, Varallo Pombia, and Pombia municipalities is reduced.

The ground trajectory projections for these new cases are reported in fig. 5.7, where there are also reported Case 1 and Case 3. Comparing Case 3 and Case 4, which consider the same take-off distance, Case 4 projection is close to Somma Lombardo. Therefore, the SEL on this municipality is greater. In addition, Case 5, as Case 3 and 4, tends to turn to the left just after take-off.

As evidenced in table 5.4 and table 5.7, for both cases previously mentioned, there is a reduction of the SEL at Somma Lombardo, the most exposed location. However, for Case 3 there is a non-negligible increase in the SEL at Borgo Ticino and Varallo Piombia, where the SEL increases 12.8% and 17.7%.

Instead, for case 4, the increase in SEL for this location corresponds to 1.6% and 7.7%,

Location	Δ SEL Case 1-4 [dB]	Δ SEL Case 1-5 [dB]
Somma Lobardo	-2.52	1.56
Vergiate	-13.11	-10.84
Arsago Seprio	-9.08	-5.38
Sesto Calende	-5.11	-4.35
Lonate Pozzolo	-0.33	-0.07
Borgo Ticino	1.04	0.35
Varallo Pombia	4.73	2.86
Pombia	3.24	1.26
Nosate	-0.86	-0.27
Molinara	-0.71	-0.04

Table 5.7: SEL difference comparison with simplified noise model

	Case 1	Case 2	Case 3	Case 4	Case 5
Average [dB]	66.28	61.74	63.03	64.01	64.79
Log-Average [dB]	72.40	66.49	68.75	67.97	70.74
Distance covered [dB]	33.23	49.32	21.55	23.5	24.22

Table 5.8: Summary of study cases results

respectively, compromising noise reduction in the locality of Somma Lombardo from 8% to 3% reduction in case 3 and case 4, respectively. Anyhow, by controlling the SEL increase at Borgo Ticino and Varallo Piombia and compromising the SEL reduction at Somma Lombardo the overall SEL reduction can be achieved.

Table 5.8 summarizes the totality of cases for Runway 35R departures. Generally, all the routes reduce the log-average of the SEL. For the same scenario configuration, an overall 1.12% SEL log-average reduction was achieved using the simplified noise model. .

Two last cases were established to further study the differences due to the introduction of the new noise model. These cases present a different scenario based on the runway 17R takeoff procedure; the route parallel to the one studied so far with takeoff in the other direction.

This configuration makes it possible to analyze the SEL in the communities located south of the airport.

In this case, the starting point is set at 45.644° latitude and 8.718° longitude, corresponding to the brake release point of runway 17R. The endpoint is set at 45.647° latitude and 9.0491° longitude, corresponding to the eastbound takeoff procedure based on SRN5W SID. In this study, the comparison concerning the current route according to SID was not

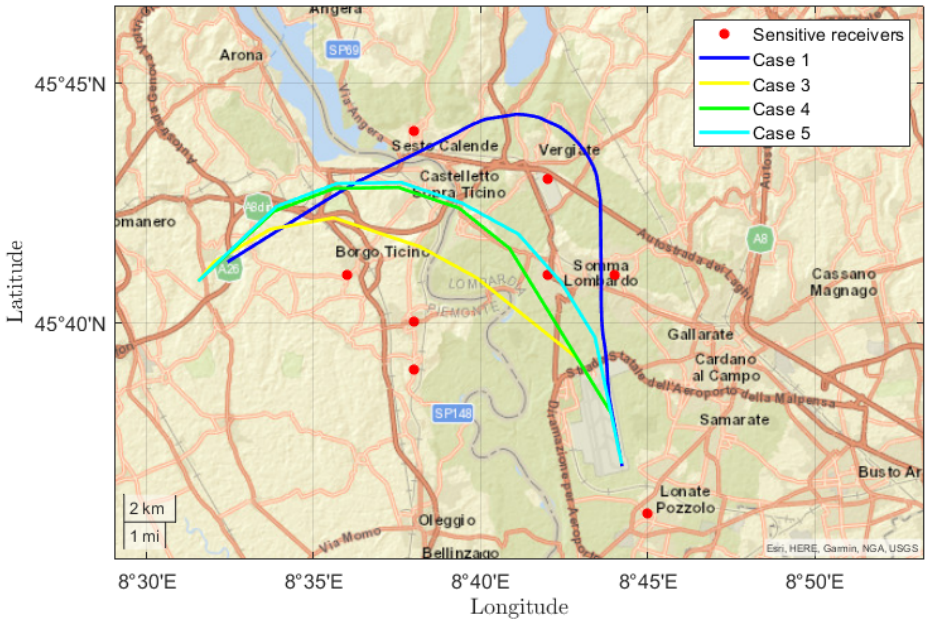

Figure 5.7: Comparison of ground track projection for optimal result with the simplified noise model

made because the objective was only to study the impact of the change of the considered noise model.

The cases studied consider an initial segment distance of 2 km, while the distance of the subsequent segments is 2.5 km. It was then defined the following cases:

Case 6 Runway 17R departure with final direction to the east with the spherical spreading noise model.

Case 7 Runway 17R departure with final direction to the east with a simplified noise model.

The results of this analysis are reported in table 5.9. In this case, Lonate Pozzolo and Castano Primo are the municipalities with the higher SEL. This table also reports the mean of each case where it is evident that the optimal solution found with the simplified model has a lower log average, improving 1.51% with respect to the inverse square law.

Figure 5.8 reports the difference in the projection to the ground of these two routes, where, both routes do not have a considerable variation in the path followed.

The introduction of this model does not significantly change the flight path, but it tends to avoid the sharp turn just after takeoff. In both cases studied, the decrease in the log average of the SEL averages 1.32%.

Location	Case 6 SEL [dB]	Case 7 SEL [dB]
Castano Primo	80.42	78.98
Lonate Pozzolo	80.23	81.06
Molinara	75.87	72.29
Robecchetto con Induno	75.18	70.60
Nosate	74.88	72.22
Inveruno	71.35	68.04
Ponte Castano	69.36	66.85
Turbigo	68.15	65.28
Cuggiono	64.27	60.92
Somma Lombardo	51.11	50.59
Average	**71.08**	**68.68**
Log-Average	**75.43**	**74.28**
Distance covered	**34.97**	**32.88**

Table 5.9: SEL case comparison for simplified noise model vs spherical spreading

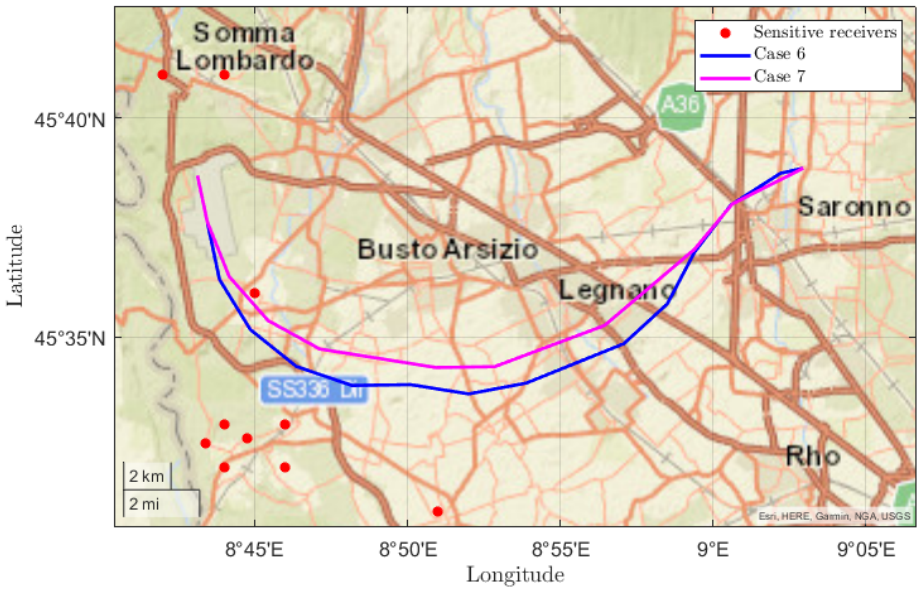

Figure 5.8: Comparison of ground track projection for case 6 and case 7

6 | Setup for data acquisition

This work used simulation for the definition of a simplified model, meanwhile the reference models from the literature have used measured data for the model's definition. Part of this thesis work was limited due to the impossibility of accessing and analyzing noise measurements. With access to this data type, further analysis and validation could have been performed. In particular, the validation of the ECAC guidelines under a real scenario and the definition of a simplified noise model from regression over measured data.

Future developments to increase the robustness of the research main's goals will depend on validating the simplified model developed, and the ECAC procedure implemented. Therefore, the next steps of the research should focus on developing tools for data acquisition to then be post-processed. In this line, the sound pressure level time-history and the precise aircraft position in time correspond to the data needed for noise assessment.

In this chapter, a preliminary research is presented and discussed to introduce the foundations for developing future work. The goal is to develop an embedded system that measures sound pressure level for an aircraft flyover and tracks its position.

Advances in technology have made smaller and modern portable computers possible. Such devices have at least one processor unit (CPU), memory unit, input/output peripheral devices, and storage disks. These are the essential components needed to create an embedded system (ES), which is a system dedicated to completing a specific task or function.

The Raspberry Pi (RP) board is a powerful compact computer capable of hosting a complete operational system (OS), which enables it to fulfill a universe of assignments[45]. The RP's relatively low-cost positions it advantageously as an ES for engineering. Therefore, it presents a viable option for the system to be developed, this choice is supported by different studies that demonstrate the feasibility of making a noise level meter with a Raspberry Pi [46].

The following proposal of an embedded system for an experimental setup is defined over the base that an RP board will be used.

6.1. Methodology

The data acquisition and analysis can be divided into three main blocks, each presenting its challenges. These three blocks correspond to the sound pressure level measurements, aircraft tracking, and the last one, the synchronization of both blocks to characterize aircraft movement regarding noise level and its position. The blocks are described below, and potential challenges for their development and implementation are detailed.

6.1.1. Sound level meter

The goal is to develop a sound level meter capable of being easily transported to different locations for data acquisition. The development of this device comprehends the selection of hardware components and the development of software ones. For the analyses expected to be performed, the following requirements are defined for the device.

- Measure SPL and reports its in dBA
- Detect aircraft flyover
- Save data for post-processing analysis
- Be easy to transport
- Minimal obstruction and background noise contamination

After the requirements definition, a preliminary development analysis was performed to detect potential challenges on its implementation. These challenges comprehend hardware, software, and procedure components and are listed and described below.

Device power supply: As the device is expected to be used in different locations, it is not dictated that there will always be a power supply available. Therefore, depending on where the measurements will be held, operating the system with a power bank would be necessary. Then, the power bank should energize the system for the necessary time. This aspect can limit the duration of the experimental measurement campaigns, so the power bank characteristics should be selected according to the measurement strategy.

Noise measurement hardware: Special attention will have to be put in selecting the microphone to use. Different factors have to be considered for selecting these hardware components. One of these corresponds to the dynamic range. The dynamic range is defined as the range between the lowest and the highest level that the microphone can handle [47]. This is not only a function of the microphone alone

but also of the preamplifier used with the microphone. The dynamic range of a microphone is, to a large extent, directly linked to its sensitivity. Therefore, it has to be selected a microphone that is sensitive to aircraft flyover SPL range.

Another factor to have in consideration is the sampling rate of the ADC. As the Nyquist sampling theorem dictates [48], the sampling frequency must be at least double the signal's highest frequency. As human is sensitive to frequencies up to 20kHz, the sampling frequency is expected to be at least 40kHz for the posterior spectrum analysis. Van Renterghem et al. [49] studied different microphones' performance for indoor and outdoor noise monitoring over various price classes for environmental noise monitoring.

Measurement strategies: As the acquired data is expected to be used for different purposes, the location of the embedded system is essential. There is a clear trade-off between background noise and power availability. Ideally, the measurements should be made at locations with negligible background noise, so the characterization of the aircraft flyover event is straightforward. Therefore, rural locations represent the best option. However, the probability that there is no constant electricity supply is high. Limiting the time in which measurements can be made

Different studies have assessed the acoustic suitability of the location for long term noise monitoring systems, and they take into account the following aspects [50]:

- Low residual sound (maximum sound pressure level of the quietest aircraft should be at least 15 dB greater than the residual long-term-average sound pressure level)
- Measuring height to 6 m
- Relevant reflecting surfaces other than ground shall be at least 10 m away
- Elevation angle should be greater than 30 degrees
- The sector should be free of obstacles
- Weather information, minimum wind speed

Flyover detection: Another aspect to consider corresponds to the detection of the flyover event. This is useful to record only the noise data of interest for the post-processing analysis. The detection of the flyover event could be implemented in two forms. The first is to define a trigger function that starts the recording when SPL is higher than a threshold level. Another approach could be utilizing the tracking function to detect if a specific aircraft is in a range for which the SPL measurement

is characterized directly by the aircraft flyover[51].

Both approaches have their pros and cons; therefore, an evaluation of both o these measurements should be achieved.

Background noise: One of the major concerns is the background noise that can interfere with the measurements' accuracy. The background noise is not negligible for the urban area, notable for places close to hospitals or train lines. An option could be the isolation of the microphone and an eventual directionality installation for a defined interest area.

6.1.2. Aircraft positioning tracking

Literature models disposed of FDR data for post-processing synchronizing between noise and aircraft position data. Aircraft tracking position over time corresponds to necessary data in the case of further noise analysis. Despite FDR data corresponding to the more reliable tracking data, its access is limited. Another approach is to take advantage of the Automatic Dependent Surveillance-Broadcast (ADS-B) System.

ADS-B is a worldwide aviation system on 1090 MHz used by aircraft to constantly broadcast their current position, altitude, airspeed, identification, whether the aircraft is turning, climbing, or descending, category of aircraft over a radio message. This functionality is the basic level of ADS-B and is known as "ADS-B out."[52]. It relies on Global Positioning System (GPS) or any other navigation system. The system architecture is reported in fig. 6.1

The described ADS-B signals of the aircraft are free to be received. To increase aircraft security, they are broadcast signals that should be received by others "ADS-B in." Therefore, the radio messages are received mainly by air traffic control stations and all other ADS-B-equipped aircraft or ground stations within the reception range. The broadcast messages can be used for real-time flight tracking with three components: a 1090 MHz antenna suitable for the frequency range, an ADB-S receiver, and dedicated software for decoding and displaying results.

Currently, Raspberry Pi can be used for ADS-B decoding. The implementation is relatively straightforward, having free online libraries with the functions to decode data. The hardware components for implementing an ADS B receive are listed below [53].

- Raspberry pi
- Power supply

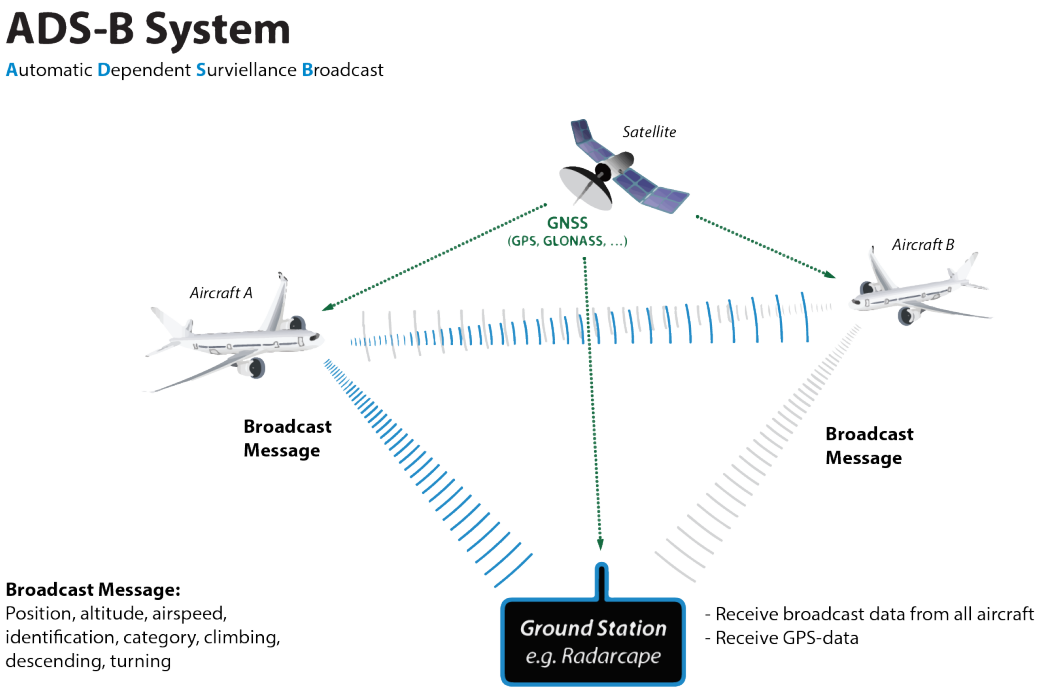

Figure 6.1: Automatic Dependent Surveillance-Broadcast working principle

Source: Jetvision [52]

- Micro Sd Card
- ASD-B USB dongle
- 1090 MHz ADS-B antenna.

6.1.3. Data synchronization

Data processing consists of synchronizing the noise recorded and the tracking data. The main goal of this step is to characterize the entire aircraft movement by the geometry between aircraft and sensitive receiver position with the respective sound pressure time-history level. With the synchronized data frame, further analyses could be performed to validate the ECAC model and the defined reduced model.

The synchronization of both data frames is expected to be performed using the time at which measurements were made.

Furthermore, it would be possible to perform spectral analysis and spectrograms with the noise characterization data. With these data available, further analyses than the validation of the previously mentioned models could be performed, such as simplified noise models based on spectral analyses for different aircraft models or classes.

7 | Conclusions and future developments

The main objective of this thesis was to find an aircraft noise model that allows to better estimate the sound level of a receiver on the ground due to aircraft flyover events. This last is to improve the performance of the NOICE model, which until the beginning of the thesis, estimated aircraft sound level assuming a single monopole source with spherical propagation that obeys the inverse square law.

In order to obtain this simplified model, preliminary research on the current aircraft noise models was performed, focusing on the so-called *best practice models*. Therefore, it was found that the models' with similar characteristics to the desired ones correspond to empirical models based on regressions from actual measurements. Specifically, these models performed regressions after frequency analysis of the measurements.

It was not possible to access actual measurements to define the model through regressions, consequently, a simulation-based approach was tried for data acquisition. The simulations were based on the implemented ECAC guidelines in compliance with the Doc. 29. For simulations, it was necessary to define a scenario representing a trajectory followed by an aircraft in a departure or arrival procedure. Then, according to the defined trajectory, L_{max} and SEL can be calculated for a specific on-ground sensitive receiver.

The objective of the simulations was to obtain measurements that would allow testing a regression model based on those found in the literature, in this case, the FLULA 2 model. In this way, by knowing the slant distance and the radiation angle between the aircraft trajectory and the on-ground sensitive receiver, the OASPL can be computed.

The scenarios defined for these simulations were based on take-off procedures of an Airbus A320. Thus, a set of on-ground receivers was defined on which the measurements were performed.

The first approach attempted to mimic what would be the time-history measurement of the SPL. To do this, L_{max} was calculated and used for each segment of each sensitive

receiver for regression. When the result was compared to that expected from the literature, noticeable differences were evident, especially in the shape of the directivity patterns.

Therefore, a second approach was tired, in which for each sensitive receiver, only L_{max} measurement is considered for the complete trajectory. Comparing the result with the literature, a better result was obtained than in the previous approach. However, for the obtained regression the directivity pattern acquired an unexpected shape with increasing the slant distance.

For the implementation, it was decided to use a piecewise function that uses the regression results up to 4000ft of slant distance. For larger distances, it considers the propagation according to the inverse square law with a correction factor due to the unmodeled attenuation effect. For distances greater than 13000ft, an SPL equivalent to a rural environment is defined.

Despite not having been able to validate the model with measurements, a case studies analysis was carried out to preliminary evaluate the performance of the NOICE model and evaluate the change of the optimal route according to how the ground receivers perceive the noise level is modeled.

The scenario used for the case studies was Milano Malpensa airport. Specifically, the study compared the optimal routes resulting from the optimization with the current noise abatement procedures implemented by SEA, the airport operator.

When analyzing these routes, it was found that noise exposure at the most impacted locations decreased on average. However, decreases in noise exposure at certain locations lead to increases at other locations. Nevertheless, the overall exposure at the most impacted locations decreases.

A not minor problem was identified when analyzing the results of the optimal route in the current scenario corresponding to the airport. Where an optimal route crosses or passes over the runway parallel to the one studied, a situation that may imply a decrease in flight and procedural safety.

Although at the time this thesis work is completed, the NOICE program is still under development and is not a tool with direct application. The analysis of the case studies shows the importance of validating the results obtained from the NOICE program at what would be the potential application site. These analyses also provide input to the application of the optimization tool that could be useful in improving the overall robustness of the NOICE model, even when all the results of the tool need to be validated. Therefore, it is suggested that the NOICE analysis for optimal routes preliminarily assess the intrinsic

constraints of the application scenario.

When comparing the results of the optimization tool depending on the sound model used, no significant changes in the optimal route were evident. However, for the cases studied, the new sound model decreases the log-average of the SEL by 1.31%.

As for the increase in computation time, 60 times slower is a significant relative difference, but could be accepted in absolute terms. Therefore, if the number of times to compute the SPL is still contained, the use of the simplified model can be recommended, but continuous improvement of the performance of the optimization algorithm is crucial. In addition, it is possible to improve or try other approaches to obtain a simplified noise model.

Finally, the next steps of the research will depend on the availability and analysis of actual measurements. Thus, the proposed future work focuses on the conceptual development of an integrated data collection system. This concept encompasses three important phases identified in the data collection phase. These correspond to the development of the sound level meter, the tracking of the aircraft and the synchronization of the two data sets. Although the proposal presented is only a conceptual proposal that will be developed in the future. A preliminary analysis of the future development challenges of this system has been presented.

With the experimental data, it is expected to validate the implementation of the ECAC model, validate the current model or even test new approaches to obtain the model. An understudied approach with excellent development potential, using large data sets, corresponds to machine learning with neural networks to estimate ground level aviation noise according to a defined trajectory.

Bibliography

[1] M. Basner, C. Clark, A. Hansell, J. Hileman, S. Janssen, K. Shepherd, and V. Sparrow, "Aviation Noise Impacts: State of the Science," *Noise and Health*, vol. 19, pp. 41–50, Mar. 2017. Publisher Copyright: © 2017 Noise & Health | Published by Wolters Kluwer - Medknow.

[2] V. Sparrow, T. Gjestland, R. Guski, I. Richard, M. Basner, A. Hansel, Y. De Kluizenaar, C. Clark, S. Janssen, V. Mestre, A. Loubeau, A. Bristow, S. Thanos, M. Vigeant, and R. Cointin, *Aviation Noise Impacts White Paper: State of the Science 2019: Aviation Noise Impacts*, pp. 44–61. Sept. 2019.

[3] T. Münzel, F. P. Schmidt, S. Steven, J. Herzog, A. Daiber, and M. Sørensen, "Environmental noise and the cardiovascular system," *Journal of the American College of Cardiology*, vol. 71, no. 6, pp. 688–697, 2018.

[4] IATA, "20 year passenger forecast." `https://www.iata.org/en/publications/store/20-year-passenger-forecast/`. (Accessed on 02/01/2022).

[5] E. E. Agency, "Exposure of europe's population to environmental noise - european environment agency." `https://www.eea.europa.eu/data-and-maps/indicators/exposure-to-and-annoyance-by-2/assessment-4`. (Accessed on 02/01/2022).

[6] ICAO, "Aircraft Noise, Balanced Approach to Aircraft Noise Management." `https://www.icao.int/environmental-protection/pages/noise.aspx#:~:text=The%20Balanced%20Approach%20consists%20of,elements%2C%20described%20in%20Figure%201.` (Accessed on 02/01/2022).

[7] ICAO, "Reduction of noise at source." `https://www.icao.int/environmental-protection/Pages/Reduction-of-Noise-at-Source.aspx`. (Accessed on 02/01/2022).

[8] ICAO, "Land-use planning and management." `https://www.icao.int/environmental-protection/Pages/Land-use-Planning-and-Management-.aspx`. (Accessed on 02/01/2022).

[9] ICAO, "Noise abatement operational procedures." https://www.icao.int/environmental-protection/Pages/Noise-Abatement-Operational-Procedures.aspx. (Accessed on 02/01/2022).

[10] ICAO, "Operating restrictions." https://www.icao.int/environmental-protection/Pages/Operating-Restrictions.aspx. (Accessed on 02/01/2022).

[11] M. Gullo, "Air trajectory optimization for noise reduction," Master's thesis, Politecnico di Milano, Milano, 2021.

[12] Soundproofing Company, "What is sound?." https://www.soundproofingcompany.com/soundproofing_101/what-is-sound. (Accessed on 01/20/2022).

[13] C. J. Plack, "Auditory perception," in *Handbook of Cognition*, pp. 71–104, 1 Oliver's Yard, 55 City Road, London EC1Y 1SP United Kingdom: SAGE Publications Ltd, 2013.

[14] Siemens, "Octaves in human hearing." https://community.sw.siemens.com/s/article/octaves-in-human-hearing. (Accessed on 01/20/2022).

[15] Siemens, "What is A-weighting?." https://community.sw.siemens.com/s/article/what-is-a-weighting. (Accessed on 01/20/2022).

[16] FAA, "Fundamentals of noise and sound." https://www.faa.gov/regulations_policies/policy_guidance/noise/basics/. (Accessed on 03/20/2022).

[17] ICAO, *Environmental technical manual*, vol. 1. Procedures for the Noise Certification of Aircraft. Montreal, Quebec: International Civil Aviation Organization, 2018.

[18] U. Isermann and L. Bertsch, "Aircraft noise immission modeling," *CEAS Aeronaut. J.*, vol. 10, pp. 287–311, Mar. 2019.

[19] S. R. More, *Aircraft noise characteristics and metrics*. Purdue University, 2010.

[20] L. Bertsch, D. G. Simons, and M. Snellen, "Aircraft noise: The major sources, modelling capabilities, and reduction possibilities," tech. rep., 2015.

[21] D. K. Wilson, C. L. Pettit, and V. E. Ostashev, *Sound propagation in the atmospheric boundary layer*. Acoustical Society of America, 2015.

[22] K. Attenborough, "Sound propagation in the atmospheric boundary layer," in *Springer Handbook of Acoustics*, pp. 117–155, New York, NY: Springer New York, 2014.

[23] A. Vela and S. Y. Oleyaei-Motlagh, "Ground level aviation noise prediction: A sequence to sequence modeling approach using lstm recurrent neural networks," pp. 1–8, 10 2020.

[24] ECAC, "Report on standard method of computing noise contours around civil airports. 4th edition volume 1: Applications guide." `https://www.ecac-ceac.org/images/documents/ECAC-Doc_29_4th_edition_Dec_2016_Volume_1.pdf`, 10 2016. (Accessed on 02/28/2022).

[25] European Union, "Directive 2002/49/ec of the european parliament and of the council of 25 june 2002 relating to the assessment and management of environmental noise," *OJ*, vol. 45, 2002.

[26] European Union, "Directive 2009/12/ec of the european parliament and of the council of 11 march 2009 on airport charges.," *OJ*, vol. 52, 2009.

[27] ICAO, "Doc 911. Recommended Method for Computing Noise Contours Around Airports. Second Edition," 2018.

[28] FAA, "Integrated noise model (INM) version 7.0 technical manual." `https://rosap.ntl.bts.gov/view/dot/12188`, 1 2008. (Accessed on 03/21/2022).

[29] FAA, "Aviation Environmental Design Tool (AEDT)." `https://aedt.faa.gov/`. (Accessed on 03/21/2022).

[30] S. Pietrzko and R. Bütikofer, "Flula-swiss aircraft noise prediction program," 01 2002.

[31] B. Schäffer, "Empa - Acoustics/Noise Control - FLULA2." `https://www.empa.ch/web/s509/flula2`. (Accessed on 02/25/2022).

[32] R. Mieskoski, "Capturing and modeling a three-dimensional stationary noise source directivity pattern with a dynamic array in the near field," Master's thesis, Department of Physics, Wright State University, 2013.

[33] J.-M. Wunderli, "Empa - Acoustics/Noise Control - sonAIR." `https://www.empa.ch/web/s509/sonair`. (Accessed on 02/25/2022).

[34] J. Meister, S. Schalcher, J.-M. Wunderli, D. Jäger, C. Zellmann, and B. Schäffer, "Comparison of the aircraft noise calculation programs sonair, flula2 and aedt with noise measurements of single flights," *Aerospace*, vol. 8, no. 12, 2021.

[35] U. Isermann and B. Vogelsang, "Azb and ecac doc.29—two best-practice european aircraft noise prediction models," *Noise Control Engineering Journal*, vol. 58, p. 455, 07 2010.

[36] ECAC, "Report on standard method of computing noise contours around civil airports. 4th edition volume 2: technical guide." https://www.ecac-ceac.org/images/documents/ECAC-Doc_29_4th_edition_Dec_2016_Volume_2.pdf, 10 2016. (Accessed on 02/28/2022).

[37] C. Zellmann, J. Wunderli, and C. Paschereit, "The sonAIR Sound Source Model: Spectral Three-Dimensional Directivity Patterns in Dependency of the Flight Condition," 08 2016.

[38] ECAC, "Report on standard method of computing noise contours around civil airports. 4th edition volume 3 part 1." https://www.ecac-ceac.org/images/documents/ECAC-Doc_29_4th_edition_Dec_2016_Volume_3_Part_1.pdf, 10 2016. (Accessed on 02/28/2022).

[39] EUROCONTROL, "The Aircraft Noise and Performance (ANP) Database : An international data resource for aircraft noise modellers." https://www.aircraftnoisemodel.org/. (Accessed on 03/08/2022).

[40] Flightradar24, "Flightradar24: Live flight tracker - real-time flight tracker map." https://www.flightradar24.com/45.5,9.26/13. (Accessed on 03/08/2022).

[41] D. Amargianitakis, R. H. Self, A. Torija, and A. Synodinos, "Influence of sound reflection on aircraft directivity and lateral attenuation on the ground," Inter.Noise 2019 Madrid, 6 2019.

[42] Assaeroporti, "Dati annuali traffico aeroportuale italiano." https://assaeroporti.com/dati-annuali/. (Accessed on 03/20/2022).

[43] SEA, "Aeroporto di Malpensa - Mappatura acustica dell'infrastruttura aeroportuale - d.lgs. 194/05," 2017.

[44] SEA, "Aeroporti di Milano Malpensa. Piano d'Azione ai sensi del D.Lgs. 194/05 SINTESI NON TECNICA," 2017.

[45] J. E. Noriega-Linares and J. M. Navarro, "On the application of the raspberry pi as an advanced acoustic sensor network for noise monitoring," *Electronics MDPI*, vol. 5, 10 2016.

[46] L. Jacomussi, W. Fonseca, and P. Mareze, "Raspberry pi: A low-cost embedded system for sound pressure level measurement," 08 2020.

[47] J. Lewis, "Understanding Microphone Sensitivity | Analog Dialogue 46-05 Back Burner." https://www.analog.com/en/analog-dialogue/articles/

understanding-microphone-sensitivity.html, 5 2012. (Accessed on 03/23/2022).

[48] C. Shannon, "Communication in the presence of noise," *Proceedings of the IRE*, vol. 37, pp. 10–21, jan 1949.

[49] T. Renterghem, P. Thomas, F. Dominguez, S. Dauwe, A. Touhafi, B. Dhoedt, and D. Botteldooren, "On the ability of consumer electronics microphones for environmental noise monitoring," *Journal of environmental monitoring : JEM*, vol. 13, pp. 544–52, 12 2010.

[50] L. B. Mª Jesús Ballesteros, "New approach to accredited noise monitoring systems according to ISO 20906," Inter.Noise 2019 Madrid, 6 2019.

[51] R. Giladi, "Real-time identification of aircraft sound events," *Transportation Research Part D: Transport and Environment*, vol. 87, p. 102527, 2020.

[52] JetVision, "What is ads-b, which requirements? - blog -." https://shop.jetvision.de/Blog/What-is-ADS-B-What-Requirements. (Accessed on 03/20/2022).

[53] FlightRadar24, "Build your own ads-b receiver - pi24 client for flight tracking | flightradar24." https://www.flightradar24.com/build-your-own. (Accessed on 03/20/2022).

A | Simplified noise model

```
def SPL(d,angle):
    """
    Parameters
    ----------
    d : Distance in feet.
    angle : Angle in degrees.
    Returns
    -------
    val : Corresponds to the sound pressure level.
    """
    a0 =       -1.02
    a1 =     0.05623
    a2 =     -0.2556
    a3 =     0.02304
    a4 =       0.388
    a5 =     -0.1536
    a6 =     -0.3262
    a7 =     -0.2076
    b0 =         148
    b1 =       -4.35
    b2 =       12.03
    b3 =       4.286
    b4 =      -0.942
    b5 =       9.581
    b6 =      -4.046
    b7 =       8.634
    c0 =    -0.00184
    c1 =   0.0003005
    c2 =     0.00157
    c3 =    -0.00181
    c4 =   -0.008654
```

```
c5 =   0.0008818
c6 =    0.009034
c7 =    0.001653
d0 =   4.366e-08
d1 =  -1.711e-08
d2 =  -5.409e-08
d3 =   1.101e-07
d4 =   6.077e-07
d5 =  -8.014e-08
d6 =   -7.14e-07
d7 =  -5.379e-08

x = angle
y = d
if y <= 4000:
    val = np.cos(np.pi*x/180)*(a1*20*np.log10(y)+b1+c1*y+d1*y**2)+
        np.cos(np.pi*x/180)**2*(a2*20*np.log10(y)+b2+c2*y+d2*y**2)+
        np.cos(np.pi*x/180)**3*(a3*20*np.log10(y)+b3+c3*y+d3*y**2)+
        np.cos(np.pi*x/180)**4*(a4*20*np.log10(y)+b4+c4*y+d4*y**2)+
        np.cos(np.pi*x/180)**5*(a5*20*np.log10(y)+b5+c5*y+d5*y**2)+
        np.cos(np.pi*x/180)**6*(a6*20*np.log10(y)+b6+c6*y+d6*y**2)+
        np.cos(np.pi*x/180)**7*(a7*20*np.log10(y)+b7+c7*y+d7*y**2)+
        (a0*20*np.log10(y)+b0+c0*y+d0*y**2)
elif y > 4000 and y < 13000 :
    delta = 3.066*(10**-8)*y**2 - 0.00161*y + 1.468
    y_s = y
    y = 4000
    val = np.cos(np.pi*x/180)*(a1*20*np.log10(y)+b1+c1*y+d1*y**2)+
        np.cos(np.pi*x/180)**2*(a2*20*np.log10(y)+b2+c2*y+d2*y**2)+
        np.cos(np.pi*x/180)**3*(a3*20*np.log10(y)+b3+c3*y+d3*y**2)+
        np.cos(np.pi*x/180)**4*(a4*20*np.log10(y)+b4+c4*y+d4*y**2)+
        np.cos(np.pi*x/180)**5*(a5*20*np.log10(y)+b5+c5*y+d5*y**2)+
        np.cos(np.pi*x/180)**6*(a6*20*np.log10(y)+b6+c6*y+d6*y**2)+
        np.cos(np.pi*x/180)**7*(a7*20*np.log10(y)+b7+c7*y+d7*y**2)+
        (a0*20*np.log10(y)+b0+c0*y+d0*y**2)
    val = val + 20*np.log10(y/y_s) + delta
else:
    val = 40
return val
```

Acknowledgements

I can't end this stage of my life without being grateful. Without the support of many people, today I could not be finishing this thesis in a country where I would never imagine ending when I started university. It has been a long journey, where I have learned through failures and successes.

I want to especially thank my thesis supervisor, Mr. Matteo Crippa(28+?), who, with his unique personality, has made me learn through constantly questioning the results I reach, and that the secret of eternal youth is loving your work. Beyond his support as a tutor, I appreciate his time and dedication to making me grow as a person and as a future professional. Also, to Francesco Gritta, my co-supervisor at TXT, who was always willing to listen to my doubts and concerns and find the right words, not to give me the answer, but for providing me the guidance to arrive at them.

I also thank my supervisor Professors: Professor Alberto Rolando, for whom I have a special appreciation since it was the teacher with whom I took my first course in Italian and despite the first classes understand almost nothing, was fundamental in taking the next step in learning Italian, and to Professor Carlo Riboldi who guided the academic work and were always available to answer my questions.

Throughout this process, the support of my family, especially my parents and siblings, was of vital importance. I believe that if it were not for them, I would never have gotten to where I am now. Beyond the financial support, the psychological and emotional support they gave me, being near or far from home and that I once needed, was crucial. Thanks for always motivating me to show the best of myself and making me understand that dreams and goals are to be pursued.

I thank all the friends I have made in these long 9 years of university. Also, to whose, however momentary I have known, were part of my university life. Whether you have met them in Chile or Italy, I believe that an essential part of life is interpersonal relationships with others. I do not forget my friends from school, who continue to support me despite distance and time. Thank you all for your good company on those hard nights of study and partying, which served to make the college years the best of my life.

I thank TXT for allowing me to develop my thesis in its facilities. The environment in which I performed my thesis was amicable and stimulating. I greatly appreciate the cultural exchange that I could develop in the company.

Finally, like the song by Violeta Parra *Gracias a la Vida* (thanks to life) that has carried me through the great learning experiences that I have had so far.